VŠB – Technical University of Ostrava
Faculty of Electrical Engineering and Computer Science
Department of Computer Science

Movement character analysis of the Belousov-Zhabotinsky reaction on parameter dependence

Analýza charakteru pohybu Bělousovova–Žabotinského modelu v závislosti na parametru

2020 Judita Nagyová

VŠB - Technical University of Ostrava
Faculty of Electrical Engineering and Computer Science
Department of Applied Mathematics

Diploma Thesis Assignment

Student: **Bc. Judita Nagyová**

Study Programme: N2647 Information and Communication Technology

Study Branch: 1103T031 Computational Mathematics

Title: Movement character analysis of the Belousov-Zhabotinsky reaction on parameter dependence
Analýza charakteru pohybu Bělousovova–Žabotinského modelu v závislosti na parametru

The thesis language: English

Description:

There are several possibilities for describing of given dynamical system's behavior. It is possible to describe given models by differential equations and to study their dynamical properties.

The main aim of the thesis is the study of differential equations and their dynamics, mainly models of the Belousov-Zhabotinsky chemical reaction type, using appropriate methods (e.g. the 0-1 test for chaos).

The tools of the thesis:

1. study basic notions and properties,
2. application of given techniques on models of the Belousov-Zhabotinsky chemical reaction,
3. implementation of methods for detecting of dynamical properties,
4. testing of methods on given differential equations,

References:

[1] D.W. Jordan and P. Smith, Nonlinear ordinary differential equations an introduction for scientists and engineers, Oxford GB, 2011
[2] Györgyi L, Field RJ, 1992. A three-variable model of deterministic chaos in the Belousov-Zhabotinsky reaction. Nature, 355(6363): 808-810.
[3] D'Ambrosio, R., Moccaldi, M., Paternoster, B. et al. Adapted numerical modelling of the Belousov–Zhabotinsky reaction. J Math Chem (2018) 56: 2876.
[4] M. W. Hirsch, S. Smale and R. L. Devaney. Differential Equations, Dynamical Systems, and An Introductions to Chaos, 2004, Elsevier (USA)
[5] S. Lynch, Dynamical systems with Applications using Matlab, Birkhauser, 2004, ISBN: 0-8176-4321-4

Extent and terms of a thesis are specified in directions for its elaboration that are opened to the public on the web sites of the faculty.

Supervisor: **doc. RNDr. Marek Lampart, Ph.D.**

Date of issue: 01.09.2019

Date of submission: 30.04.2020

prof. RNDr. Jiří Bouchala, Ph.D.
Head of Department

prof. Ing. Pavel Brandštetter, CSc.
Dean

I hereby declare that this master's thesis was written by myself. I have quoted all the references I have drawn upon.

Ostrava, May 1, 2020 .....

I would like to thank everybody who supported me in writing this thesis. Especially, my sincere thanks go to my supervisor doc. RNDr. Marek Lampart, Ph.D., for his help, patience and motivation.

Abstrakt

Hlavním cílem této práce je zkoumat dynamické vlastnosti Györgyi-Fieldova modelu Belousov-Žabotinského chemické reakce. Odpovídající model o třech proměnných je zadaný soustavou nelineárních obyčejných diferenciálních rovnic závislých na jednom parametru, který označuje průtok. Protože některé hodnoty tohoto parametru mohou vést k chaosu, byla provedena analýza za účelem identifikace různých dynamických režimů. Dynamické vlastnosti byly kvalifikovány a kvantifikovány klasickými i novými technikami, jako jsou fázové portréty, bifurkační diagram, Fourierova spektrální analýza, 0-1 test na chaos a aproximační entropie. Podrobně byla zkoumána korelace mezi aproximační entropií a 0-1 testem chaosu. Navíc byl zkonstruován systém tří vnořených podintervalů parametru průtoků, pro který byl v každé úrovni vypočítán 0-1 test na chaos a aproximační entropie, které měly stejnou strukturu. Studie vede k otevřenému problému, zda množina parametrů průtoku má strukturu podobnou Cantorově množině.

Klíčová slova: Belousov-Žabotinského reakce; Györgyi-Fieldův model; 0-1 test chaosu; aproximační entropie; bifurkace

Abstract

The main aim of this thesis is to detect dynamical properties of the Györgyi-Field model of the Belousov-Zhabotinsky chemical reaction. The corresponding three-variable model given as a set of nonlinear ordinary differential equations depends on one parameter, the flow rate. As certain values of this parameter can give rise to chaos, the analysis was performed in order to identify different dynamics regimes. Dynamical properties were qualified and quantified using classical and also new techniques. Namely, phase portraits, bifurcation diagrams, the Fourier spectra analysis, the 0-1 test for chaos, and approximate entropy. The correlation between approximate entropy and the 0-1 test for chaos was observed and described in detail. Moreover, the three-stage system of nested subintervals of flow rates, for which in every level the 0-1 test for chaos and approximate entropy was computed, is showing the same pattern. The study leads to an open problem whether the set of flow rate parameters has Cantor like structure.

Key Words: Belousov-Zhabotinsky reaction; Györgyi-Field model; 0-1 test for chaos; approximate entropy; bifurcation

Contents

List of Figures

List of Tables

Listings

1 Introduction

The study of dynamical systems has drawn interest in many scientific fields as its techniques can be applied to solve problems from physics, biology, ecology, economics, or chemistry. The latter one involves chemical reactions, which describe a kind of a dynamical system and can be also modeled mathematically. This thesis deals with a class of reactions that are not driven by equilibrium thermodynamics, the Belousov-Zhabotinsky (BZ) reaction.

The BZ reaction was originally discovered in the 1950s by Boris P. Belousov [39] when he was studying a chemical model of the Krebs cycle. During the experiment, he observed his solution changing colours repeatedly, instead of stabilizing, which would indicate that the reaction proceeded to equilibrium. Later, in the 1960s, his work was took up by his graduate student Anatol Zhabotinsky, who confirmed his results, that oscillations may be present even in homogeneous chemical reactions. The discovery was revealed to the world in 1968 at a symposium in Prague [39].

Since then, the reaction intrigues chemists, biologists and mathematicians alike. Its chemical mechanism, though quite complex, can be described as a reaction of an organic substrate (usually malonic acid), which is oxidized by bromate ions in the presence of a transition metal ion (commonly cerium and ferroin) in an acidic solution [39]. This is described by a numerous chemical equations. To be able to study the behaviour, simplifications were made both in chemical and mathematical models, to better describe different aspects of the BZ reaction. The first commonly known model is the Brusselator, which was proposed by Prigogine and Lefever in 1968. It describes the formation of dissipative structures. Later, in 1972, Field, Körös and Noyes presented the Field, Körös and Noyes (FKN) mechanism, of which the resulting mathematical model is the Oregonator.

In the 1970s, researchers started to study the BZ reaction taking place in flow reactors, where reactants are continuously replenished into the solution by a constant flow of chemicals. These continuous-flow stirred-tank reactors (CSTR) gave rise to two new features. First, multiple steady states, where the reaction is stabilized in either reduced or oxidized state, while large perturbations may push the reaction between the two. Second is chaos, where the reaction oscillates irregularly and unpredictably [39].

In [40] the author studies the behaviour of the reaction through the Oregonator model depending on one parameter, the diffusion coefficient. It is possible to find a critical value, which splits the solution in an asymptotically stable unique solution, and a Turing instability, as well as the existence of nonconstant steady states by a bifurcation method.

In [41], using point information gain entropy to classify images of the BZ reaction leading to a contruction of a state trajectory.

The behaviour of the Brusselator model is studied in [34] in dependence of feedback loops. In their absence, there are self-replicating spots which lead to a hexagonal structure. Feedback loops induce extreme events.

In [5] an experimental use of the BZ reaction is described for the preparation of polymeric giant vesicles with controllable size.

A new model is taken into account in [16], a model of fractional-order BZ reaction. The bifurcations are studied depending on two parameters. The stability of both fractional- and integer-order systems, and the effect of slow-fast oscillations is analyzed.

In [1] the BZ reaction is used as a medium for implementation of BZ-based logical circuits. The reaction is encapsulated into vesicles. Wave formation of this excitable light-sensitive chemical medium is then analyzed, which can be interpreted as logical information, thus theis interaction creating logical gates.

Another use of the BZ medium is shown in [3] and is simulated based on the Oregonator model - the modified complete Oregonator model is used. The interactions of scroll waves with no-flux boundaries are studied based on layer thickness and intensity of illumination both by calculations and experiments.

In [15], the authors compare two polymer chains induced by the BZ reaction. Polymer chains are used to simulate living organisms by molecular machines, as they can generate motion without external stimuli. A study the self-oscillating behaviour was conducted, which can be controlled by the concentration and temperature of the reactants, which helps to design novel autonomous molecular robots.

Chaos of the BZ reaction is studied in [6]. The reaction is taking place in a closed and unstirred reactor. The model used is derived from the two variable Oregonator-diffusion system and the study analyzes the relation between chemical and spatial-temporal chaos, while both are found to originate from the reaction-diffusion-convection coupling.

Experimental evidence of chaotic oscillations in a closed well-stirred (batch) reactor is presented in [19].

The Oregonator model is used in its reduced two-variable form in [18]. The effect of applying an electric field is studied on the travelling waves of the BZ reaction. Problems as stopping and decelerating waves going towards the negative electrode, accelerating the waves propagating to the positive electrode, wave reversal and splitting were addressed in this work.

Similarly in [24], wave trains are studied through the two-variable Oregonator model. The evolution of waves is analyzed depending on numerous parameters and their values when the dynamics are unstable, then small values of a kinetic parameter are chosen to report a complex structure of individual waves which form the train.

The travelling waves are studied in [23], based on a kinetic parameter in the two-variable Oregonator model. Structures of both oxidation and reduction waves are observed.

The dynamics of the BZ reaction is studied in [25]. The reaction is modelled by a set of differential equations similar to the Oregonator. A corresponding stationary problem with diffusion is presented and existence of non-constant positive solutions are discussed.

In [2], the BZ reaction is studied as a reaction-diffusion cell with a non-smooth feedback mechanism consisting of varying concentrations at the boundary in response to those in the

centre of the cell. For both one- and two-dimensional geometries and depending on the feedback delay, stability and Hopf bifurcations were analyzed.

Chaos in the BZ reaction is simulated by a modified Oregonator model which incorporates the parameter of the reactor in [37].

Next to studies of regular and chaotic behaviour of the reaction, also intermittent type of chaos is experimentally verified in [4]. The results were supported by the reconstruction of attractors as well as the Fourier spectra and Poincaré sections.

In [12], a chemical model is developed corresponding to the experimental simulations of chaos in a CSTR at low flow rates. The continuation of this work can be found in [11], where the model is simplified. The original which contained 11 variables had been reduced to a 3-variable model.

The thesis is organized as follows: in Section 2, chemical reactions are introduced together with the chemical process describing the BZ reaction. The set of corresponding differential equations in presented in Section 3. The tools used for quantifying and qualifying dynamical behaviour of the system are listed in Section 4. The main results obtained by phase portraits, the Fourier spectra analysis, the approximate entropy, and the 0-1 for chaos, are contained in Section 5. Matlab scripts for the aforementioned tools are in Section 6. Finally, the outcomes are summarized in Section 7. The thesis ends with appendices where the copy of the submitted paper is given for completeness and confirmation of submission to the Jimp-type journal (Journal of Mathematical Chemistry Q2).

2 Chemical reaction modelling

Chemical reactions are part of our everyday life, forming processes like rusting, combustion, cooking, digestion or photosynthesis. In this section, chemical reactions as the mechanism of transformation of certain chemical substances into new ones is described. The chemical aspects of the BZ reaction, as an example of an oscillating chemical reaction, are analyzed.

2.1 Kinetics of chemical reactions

There are three groups of chemical species present in the reaction. The reactants, which are present in large concentrations at the beginning of the reaction, and their concentration decrease overtime. The products, which may be present in very small concentrations at the beginning, and their concentrations increase with time. Finally, intermediates can be both produced and consumed during the reaction, and their concentration is small compared to that of the reactants and products. As an example, given the reaction

$$2A + B \rightarrow C + 3D, \tag{1}$$

the reactants are A and B, the products are C and D, and there were no intermediates. The dynamics of this equation (1) is given by the change of concentration of the chemical species present, and can be described as

$$-\frac{1}{2}\frac{d[A]}{dt} = -\frac{d[B]}{dt} = \frac{d[C]}{dt} = \frac{1}{3}\frac{d[D]}{dt} = k_{reaction\_rate} \times [A][B]. \tag{2}$$

Usually, chemical systems tend to one or more temporally unchanging solutions, which can be either a chemical equilibrium, or a chemical steady state, i.e. all state variables are constant, as it is described in [7]. These solutions correspond to the mathematical equilibria, where the temporal derivatives of the variables are equal to 0.

The reaction quotient for an example reaction:

$$aA + bB \leftrightarrow cC + dD \tag{3}$$

is determined as

$$RQ = \frac{[C]^c[D]^d}{[A]^a[B]^b}. \tag{4}$$

RQ has the same value, called equilibrium constant, for a particular overall chemical reaction at thermodynamic equilibrium, regardless of the initial concentrations of chemical species. However, the instantaneous RQ for an overall reaction may differ from the equilibrium constant, resulting in the reaction spontaneously evolving toward thermodynamic equilibrium. So the reactants turn into products or vice versa depending on the RQ being less or greater than the equilibrium constant, and at the rate depending on the difference between the equilibrium con-

stant and the actual RQ. For big differences, the dynamics of the system may become more complicated, resulting in Hopf bifurcation, in which the steady state is susceptible to growing perturbations, or the trajectories grow from the steady state monotonically.

Apart from the distance from equilibrium, the changes in dynamics depend quantitatively on other parameters of the system too, e.g. the values of the rate constants.

As the nonlinear dynamics of chemical reactions can be very complex, it was widely studied through the years, starting with Turing in 1952 [38] and continued by Prigogine [30], who presented a simple two-variable model in 1968, which was later named the Brusselator. It was a beginning of theoretical approach to oscillating chemical reactions. However, there had been no experimental evidence of this phenomenon among homogeneous chemical reactions, and it was thought that such behaviour occurs only in heterogeneous processes. The correspondence between theory and real experiments was confirmed by the discovery of the BZ reaction.

2.2 The chemical mechanism of the BZ reaction

As it is shown in [7], the BZ reaction in its usual form is an oxidation of malonic acid by bromate ions in a sulfuric acid medium, catalyzed by cerium ions. Malonic acid and cerium ions can be substituted, but bromate ion must be present. The chemical mechanism was worked out by Field, Körös and Noyes, therefore it is called the FKN mechanism. Its inorganic part consists of two processes. Process A (5) occuring at high concentrations of $Br^-$and Process B (6) at low concentrations of Br^-.

$$Br^- + BrO_3^- + 2H^+ \leftrightarrow HBrO_2 + HOBr \quad \text{(FKN1)}$$

$$Br^- + HBrO_2 + H^+ \rightarrow 2HOBr + H_2O \quad \text{(FKN2)}$$

$$3Br^- + 3HOBr + 3H^+ \leftrightarrow 3Br_2 + 3H_2O \quad \text{(FKN3)}$$

$$5Br^- + BrO_3^- + 6H^+ \leftrightarrow 3Br_2 + 3H_2O \quad \text{(Stoichiometry FKN1 - FKN3)}$$

$$3Br_2 + 3CH_2(COOH)_2 \rightarrow 3BrCH(COOH)_2 + 3Br^- + 3H^+ \quad \text{(FKN4)}$$

$$2Br^- + BrO_3^- + 3CH_2(COOH)_2 + 3H^+ \rightarrow 3BrCH_2(COOH)_2 + 3H_2O$$

(Stoichiometry Process A)

$$HBrO_2 + BrO_3^- + H^+ \leftrightarrow 2BrO_2 + H_2O \quad \text{(FKN5)}$$

$$2(Ce(III) + BrO_2 + 2H^+ \leftrightarrow Ce(IV) + HBrO_2) \quad \text{(FKN6)}$$

$$HBrO_2 + BrO_3^- + 3H^+ + 2Ce(III) \leftrightarrow 2Ce(V) + 2HBrO_2 + H_2O$$

(Stoichiometry FKN5 - FKN6)

$$HBrO_2 + HBrO_2 \rightarrow HOBr + BrO_3^- + H^+ \quad \text{(FKN7)}$$

$$4Ce(III) + BrO_3^- + 5H^+ \leftrightarrow 4Ce(IV) + HOBr + 2H_2O \qquad \text{(Stoichiometry Process B)}$$

$$HOBr + CH_2(COOH)_2 + H^+ \rightarrow BrCH(COOH)_2 + H_2O \qquad \text{(FKN8)}$$

$$CH_2(COOH)_2 + 6Ce(IV) + 2H_2O \rightarrow 6Ce(III) + HCOOH + 2CO_2 + 6H^+ \qquad \text{(FKN9)}$$

$$4Ce(IV) + BrCH_2(COOH)_2 + 2H_2O \rightarrow 4Ce(III) + Br^- + HCOOH + CO_2 + 5H^+ \qquad \text{(FKN10)}$$

The critical value of $[Br^-]$ is given by

$$[Br^-]_{crit} = \frac{k_{FKN5}}{k_{FKN2}}[BrO_3^-].$$

At this point, Process A (5) shifts to Process B (6), as the reaction FKN5 dominates over reaction FKN2.

The common feature of oscillating chemical reaction is visible in Stoichiometry FKN5 - FKN6, where we can observe the autocatalysis of a molecule of $HBrO_2$ generating two molecules of $HBrO_2$. Autocatalytic Process B (6) reaches a steady state with reaction FKN7 and yields the stoichiometry Stoichiometry Process B. By FKN8, $HOBr$ is quickly removed. The reaction (7) form Process C, which involves intermediates, as e.g. products of partially oxidized organic radicals. Process C also resets the BZR cycle by reducing $Ce(IV)$ back to $Ce(III)$.

2.3 The Oregonator model

The mechanism described above can be reduced into a three-variable model by assuming the basic dynamics of the full model and modifying the values of the rate constants [7]. Process A is reduced into (8), Process B is reduced into (9), and Process C into (10).

$$BrO_3^- + Br^- \rightarrow HBrO_2 + BrMA \qquad \text{(8a)}$$

$$HBrO_2 + Br^- \rightarrow 2BrMA \qquad \text{(8b)}$$

$$2Ce(III) + HBrO_2 + BrO_3^- \rightarrow 2Ce(IV) + 2HBrO_2 \qquad \text{(9a)}$$

$$HBrO_2 + HBrO_2 \rightarrow BrMA + BrO_3^- \qquad \text{(9b)}$$

$$Ce(IV) \rightarrow fBr^- \tag{10a}$$

Substituting the chemical species present as $A = BrO_3^-$, $P = BrMA$, $X = HBrO_2$, $Y = Br^-$ and $Z = Ce(IV)$, and the rate constants $k_{O1} = k_{fkn1}$, $k_{O2} = k_{fkn2}$, $k_{O3} = k_{fkn5}$ and $k_{O4} = k_{fkn7}$, the Oregonator model is given by (11).

$$A + Y \rightarrow X + P \tag{O1}$$
$$X + Y \rightarrow 2P \tag{O2}$$
$$A + X \rightarrow 2X + Z \tag{O3}$$
$$X + X \rightarrow A + P \tag{O4}$$
$$Z \rightarrow fY \tag{O5}$$

The expendable parameters are k_{O5} and f, is the stoichiometric coefficient determining the amount of $[Br^-]$ produced per $Ce(IV)$ consumed.

The differential equation corresponding to (11) are (12).

$$\frac{dX}{dt} = k_{O1}AY - k_{O2}XY + k_{O3}AX - 2k_{O4}X^2 \tag{12a}$$
$$\frac{dY}{dt} = -k_{O1}AY - k_{O2}XY + fk_{O5}Z \tag{12b}$$
$$\frac{dZ}{dt} = k_{O3}AX - k_{O5}Z \tag{12c}$$

The steady states of the Oregonator model has been investigated using k_{O5} and f as bifurcation parameters and regions of both stable and unstable steady states were identified.

2.4 Chaos in the BZ reaction

The BZ reaction was the most studied oscillatory reaction when it came to searching for chemical chaos. However, in during experiments in any closed batch reactor, the reaction approached equilibrium. As chaos occurs only far from equilibrium, the experiments were implemented in a CSTR. These reactors are defined by a constant flow of chemical species pumped in and out of the reactor at a particular flow rate. It can maintain the reaction in a specific distance from the equilibrium in a true steady state. The flow rate parameter is defined as

$$k_f[s^{-1}] = \frac{\text{experimental flow rate } [mL\ s^{-1}]}{\text{reactor volume } [mL]}.$$

Table 1: Rates and rate constants of the GF model chemical scheme.

Reaction equation	Rate r_i	Rate constant k_i
(13a)	$r_1 = k_1 HYX$	$k_1 = 4.0 \times 10^6\, M^{-2}s^{-1}$
(13b)	$r_2 = k_2 AH^2Y$	$k_2 = 2.0\, M^{-3}s^{-1}$
(13c)	$r_3 = k_3 X^2$	$k_3 = 3000\, M^{-1}s^{-1}$
(13d)	$r_4 = k_4 A^{0.5} H^{1.5}(C-Z)X^{0.5}$	$k_4 = 55.2\, M^{-2.5}s^{-1}$
(13e)	$r_5 = k_5 XZ$	$k_5 = 7000\, M^{-1}s^{-1}$
(13f)	$r_6 = \alpha k_6 ZV$	$k_6 = 0.09\, M^{-1}s^{-1}$
(13g)	$r_7 = \beta k_7 MZ$	$k_7 = 0.23\, M^{-1}s^{-1}$

The dynamics of the reaction is observed depending of various values of the parameter k_f, expecting to be closer to the equilibrium at low values, and far from equilibrium at highr values of k_f.

2.5 The Györgyi-Field model

The GF model of the BZ reaction develops a description of the reaction in terms of a set of differential equations containing only three variables. In common with experiments, the GF model shows both regular, intermittent and chaotic behavior. While remaining close to a real chemical system, it is sufficiently simple to allow detailed mathematical analysis [10]. The mechanism of the reaction is defined by the set of the following equations (13):

$$Y + X + H \rightarrow 2V \tag{13a}$$
$$Y + A + 2H \rightarrow V + H \tag{13b}$$
$$2X \rightarrow V \tag{13c}$$
$$0.5X + A + H \rightarrow X + Z \tag{13d}$$
$$X + Z \rightarrow 0.5X \tag{13e}$$
$$V + Z \rightarrow Y \tag{13f}$$
$$Z + M \rightarrow \tag{13g}$$

where the corresponding chemical components are: $Y = \mathrm{Br^-}$, $X = \mathrm{HBrO_2}$, $Z = \mathrm{Ce^{4+}}$, $V = \mathrm{BrCH(COOH)_2}$ or BrMA, $A = \mathrm{BrO_3^-}$, $H = \mathrm{H^+}$, $M = \mathrm{CH_2(COOH)_2}$. The concentrations of the main reactants A, H, M, and the total concentration of cerium ions C are summarized in Table 2.

3 Mathematical model

The dynamics of chemical reaction is usually driven by differential equations containing nonlinear terms and feedback loops. A three-variable mathematical model of the BZ reaction, presented by Györgyi and Field in [10], describes the reaction taking place in a CSTR. The corresponding set of nonlinear ordinary differential equations contains only three variables, while still being able to accurately reproduce the behavior of the BZ reaction observed experimentally [10] and it is based on a four-variable chemical mechanism (13), see [10].

The mathematical model, in its dimensionless form, consists of a set of scaled differential equations:

$$\frac{dx}{d\tau} = T_0\Bigg(- k_1 H Y_0 x\tilde{y} + k_2 A H^2 \frac{Y_0}{X_0}\tilde{y} - 2k_3 X_0 x^2 + 0.5k_4 A^{0.5} H^{1.5} X_0^{-0.5}(C - Z_0 z)x^{0.5} - \tag{14a}$$

$$- 0.5k_5 Z_0 xz - k_f x\Bigg)$$

$$\frac{dz}{d\tau} = T_0\left(k_4 A^{0.5} H^{1.5} X^{0.5}\left(\frac{C}{Z_0} - z\right)x^{0.5} - k_5 X_0 xz - \alpha k_6 V_0 zv - \beta k_7 Mz - k_f z\right) \tag{14b}$$

$$\frac{dv}{d\tau} = T_0\left(2k_1 H X_0 \frac{Y_0}{V_0} x\tilde{y} + k_2 A H^2 \frac{Y_0}{V_0}\tilde{y} + k_3 \frac{X_0^2}{V_0} x^2 - \alpha k_6 Z_0 zv - k_f v\right) \tag{14c}$$

where

$$\tau = \frac{t}{T_0},$$

$$x = \frac{X}{X_0},$$

$$z = \frac{Z}{Z_0},$$

$$v = \frac{V}{V_0},$$

and

$$\tilde{y} = \frac{\alpha k_6 Z_0 V_0 zv}{(k_1 H X_0 x + k_2 A H^2 + k_f)\, Y_0},$$

while t corresponding to time, X to $HBrO_2$, Y to Br^-, Z to Ce^{4+}, and V to BrMA. The rate constants and parameters used in the following computations are given in the Table 1 and 2, respectively.

The behavior of this system depends on the inverse residence time of the CSTR, the flow rate, noted k_f $[s^{-1}]$. As certain values of this parameter can give rise to chaos, the following analysis was performed in order to identify different dynamics.

Table 2: Parameters of the investigated system (14).

List of parameters
$A = 0.1$
$M = 0.25$
$H = 0.26$
$C = 0.000833$
$\alpha = 666.7$
$\beta = 0.3478$

4 Tools for dynamics detection

In this section, we present the tools, which will be used for qualifying and quantifying the dynamical properties of the model. The following tools are demonstrated on a generic example for clarity. For this purpose, the Rössler system [29] is used. It is given by a set of three ordinary differential equations:

$$\frac{dx}{dt} = -y - z, \tag{15a}$$

$$\frac{dy}{dt} = x + ay, \tag{15b}$$

$$\frac{dz}{dt} = b + z(x - c) \tag{15c}$$

where x, y and z are variables, and a, b, and c are system parameters. The parameters $b = 0.2$ and $c = 5.7$ are fixed. To see the system dynamics change, parameter a will be varying from $a = 0.1$ to $a = 0.3$.

4.1 Phase portraits

A phase portrait is a geometric representation of the trajectories of a dynamical system in the phase space. A phase space is a space in which all possible states of a system are represented. A point specified in this space specifies the state of the dynamical system, and vice versa. In the phase portrait, every axis represents a degree of freedom of the system.

Let the phase space be a finite dimensional vector space $\mathbb{R}^m$. A state is specified by a vector $\boldsymbol{x} \in \mathbb{R}^m$. Then the dynamics can be described by either an m dimensional map (discrete dynamical system) or by a system of m first-order ordinary differential equations (continuous dynamical system).

A sequence of points $\boldsymbol{x}_n$ or $\boldsymbol{x}(t)$, solving the above equations, is called a trajectory of the dynamical system, with $\boldsymbol{x}_0$ or $\boldsymbol{x}(0)$, respectively, the initial condition. Typical trajectories will either run away to infinity as time proceeds or stay in a bounded area. Examples of different shapes of Rössler system's (15) trajectories, from simple loops and regular periodic dynamics for $a = 0.1$ and $a = 0.15$, to chaotic trajectories for $a = 0.2$ and $a = 0.3$, are given in Figure 1.

4.2 Poincaré sections

This method consists of constructing a suitable oriented surface in phase space and an invertible map on this surface by following a trajectory of the dynamical system. The iterates of the map are given by the points of intersection of the surface and the trajectory in a specified direction. This results in a discrete dynamical system which also reduces the dimension of the phase space by one. The remaining points depend on both the actual trajectory, as well as on the chosen surface.

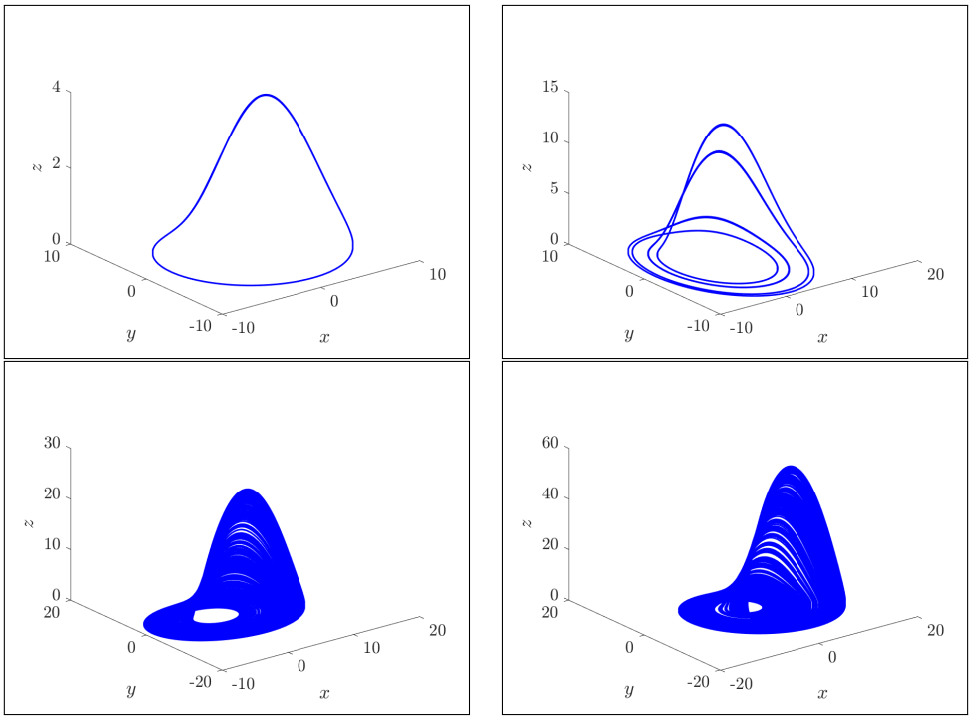

Figure 1: Examples of phase portraits of the Rössler system (15) for $a = 0.1$ (top left), $a = 0.15$ (top right), $a = 0.2$ (bottom left), and $a = 0.3$ (bottom right).

In Figure 2, different Poincaré section of the same plane and different trajectories are given for the Rössler system (15). More points of intersections arise as the dynamics of the system becomes more complex.

4.3 Fourier spectra

The Fourier transform is used to decompose a function or a signal into its constituent frequencies. It establishes a correspondence between the signal at certain times and contribution of frequencies to the signal, and how the phases of the oscillations are related to the phases of other oscillations.

The Fourier transform of a function $s(t)$ is given by

$$S(f) = \frac{1}{\sqrt{2\pi}} \int_{-\infty}^{\infty} s(t) e^{2\pi i f t} dt \tag{16}$$

and the Fourier transform of a finite discrete time series by

$$S_k = \frac{1}{\sqrt{N}} \sum_{n=1}^{N} s_n e^{2\pi i k n/N} \tag{17}$$

where the frequencies are $f_k = k/N\Delta t$, $k = -N/2, ..., N/2$, and Δt is the sampling interval. The periodic and chaotic dynamics show visibly distinct Fourier spectra. Periodic or quasi-

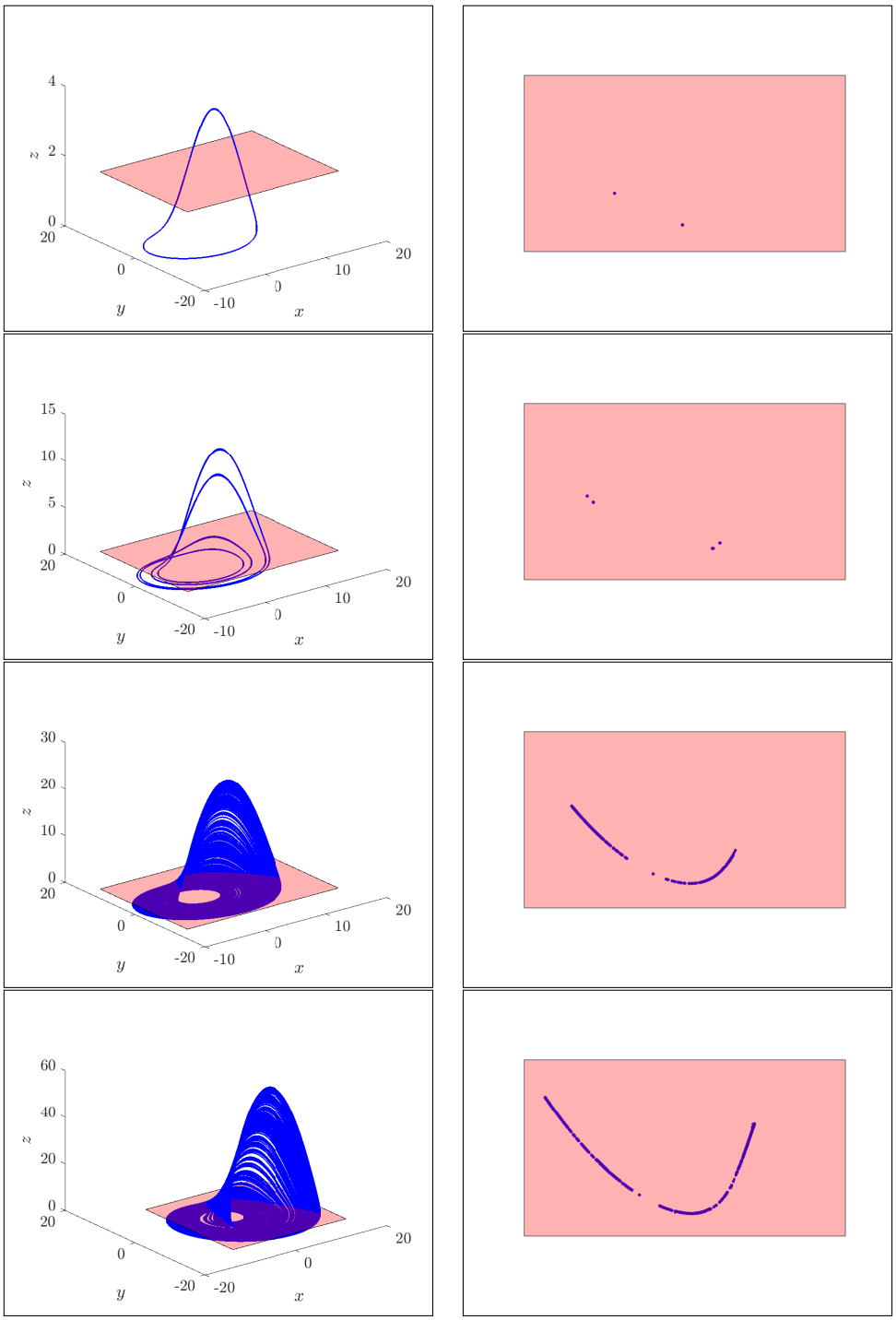

Figure 2: Examples of Poincaré sections of the Rössler system (15) for $a = 0.1$, $a = 0.15$, $a = 0.2$ and $a = 0.3$ (from top to bottom).

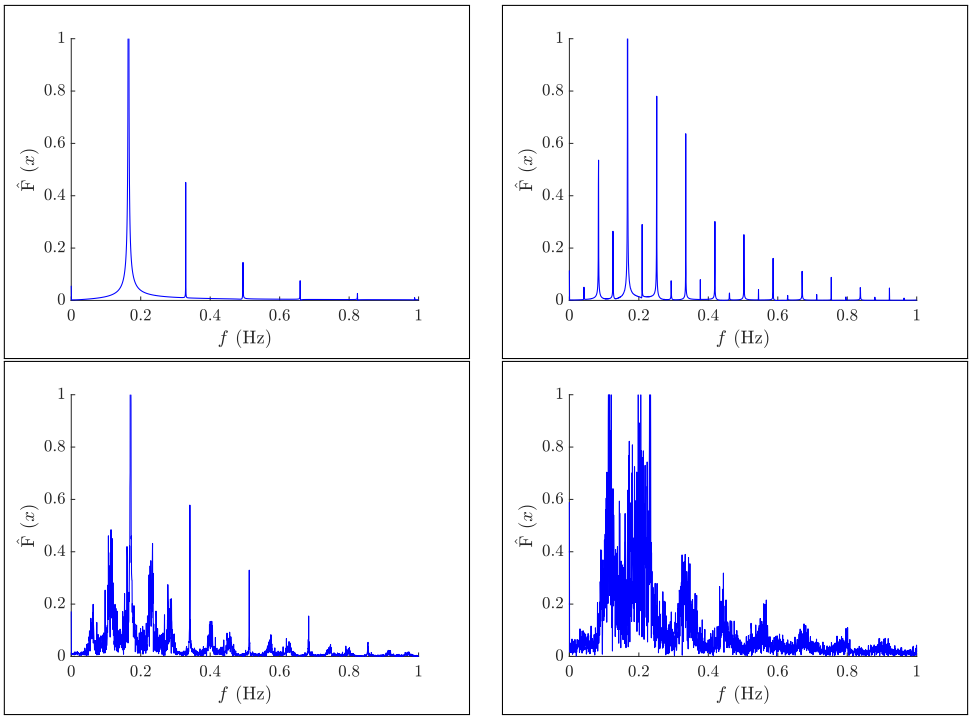

Figure 3: Examples of frequency spectra of the Rössler system (15) for $a = 0.1$ (top left), $a = 0.15$ (top right), $a = 0.2$ (bottom left), and $a = 0.3$ (bottom right).

periodic signals show sharp peaks at the dominant frequencies and at their integer multiples, the harmonic frequencies, with measurement noise adding a continuous floor to the spectrum. Chaotic signals may also have sharp spectral lines but there always exists a continuous part of the spectrum.

The difference in the frequency spectrum of the Rössler system (15), both for regular and chaotic cases, is shown in Figure 3.

4.4 Bifurcation diagram

Bifurcations are sudden changes in the geometry or topology of the system's attractor at a critical value of a parameter. The most common type is the period doubling bifurcation. At a specific critical value of the parameter, a stable orbit of period p becomes unstable, and an orbit of period $2p$ appears. This can happen multiple times with more period doublings occuring with increasing values of the parameter, until infinite period appears and the dynamics become chaotic.

The bifurcation diagram, see Figure 4, is the representation of changes that a dynamical system undergo depending on a change in its parameters. The diagram is constructed as the values visited or approached as a function of the bifurcation parameter.

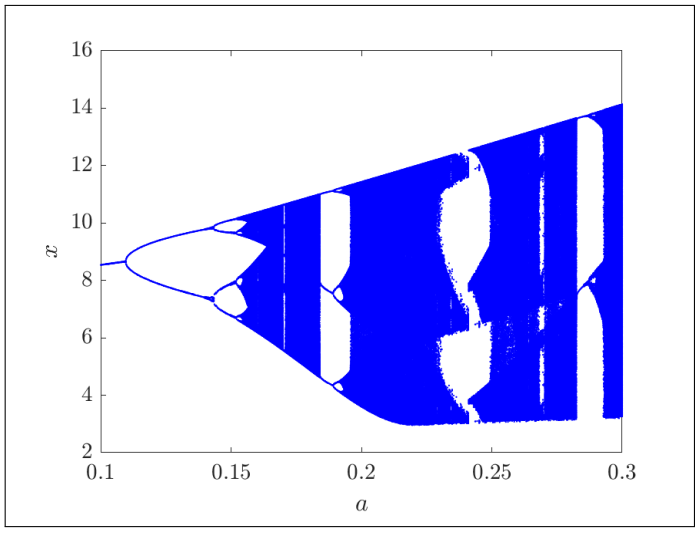

Figure 4: Example of a bifurcation diagram of the variable x of the Rössler system (15) varying a.

4.5 Approximate entropy

The approximate entropy is a technique used to quantify the amount of regularity and unpredictability of fluctuations in time-series. The main advantages are that it can be computed on short time series and it allows to compare the differences in complexity of the same system with different parameters settings, see, e.g., [28] to be detected. More complex notion of entropy type can be found in, e.g., [17].

This method is used alongside other tools for dynamics detection, e.g. in [20] to investigate the dynamics of an electric circuit, or in [14], where it is used to analyse electrophysiology of the heart. Also, an accelerated modification of the original algorithm, the fast approximate entropy, was proposed in [35].

Approximate entropy is computed using the following algorithm.

First, two parameters of the computations are set - the embedding dimension m and neighborhood threshold r. Let $u(t) \in \mathbb{R}$ for $t = \{1, 2, \ldots, N\}$ be a time series with N observations. We form a sequence of vectors $x(1), x(2), \ldots, x(N-(m-1))$ in $\mathbb{R}^m$, defined as $x(i) = [u(i), u(i+1), u(i+2), \ldots, u(i+(m-1))]$, where t is the observed time and m is the embedding dimension. The distance of embedded vectors is computed as

$$D(i,j) = d(x(i), x(j)) = \max_{k=1,2,\ldots,m} |u(i+k-1) - u(j+k-1)|, \tag{18}$$

for $i, j = \{1, 2, \ldots, N-(m-1)\}$.

The thresholded version of the distance with threshold given by r is computed by

$$d_r(i,j) = \begin{cases} 1, & D(i,j) < r \\ 0, & otherwise, \end{cases} \tag{19}$$

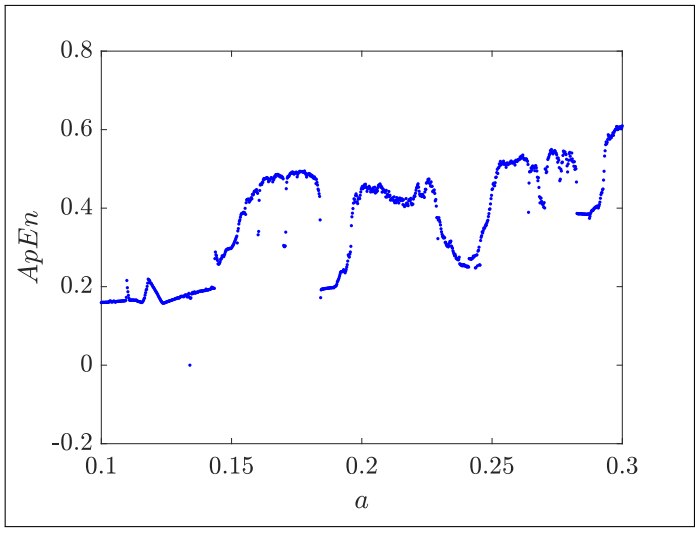

Figure 5: The results of approximate entropy for the range of parameter $a = 0.1$ to $a = 0.3$ of the Rössler system (15).

for $i, j \in \{1, 2, \ldots, N - (m-1)\}$.

The ratio $C_i^m(r)$ between points in the neighborhood of i and the number of embedded vectors is computed.

$$C_i^m(r) = \frac{\sum_{j=1}^{N-(m-1)} d_r(i,j)}{N-(m-1)}. \tag{20}$$

The average of logarithm of all the $C_i^m(r)$ is given by

$$\Phi^m(r) = \frac{1}{N-(m-1)} \sum_{i=1}^{N-(m-1)} \ln C_i^m(r). \tag{21}$$

Finally, approximate entropy for the finite time series with N data points is computed as

$$ApEn(m, r, N) = \Phi^m(r) - \Phi^{m+1}(r). \tag{22}$$

For robust estimation, it was suggested by Pincus [28] the time series is containing at least 10^3 observations.

The results of approximate entropy for parameter a from 0.1 to 0.3 of the Rössler system (15) is shown in Figure 5. In comparison to the bifurcation diagram 4, we observe increasing entropy with increasing period of the system. Approximate entropy reaches its highest values in chaotic regions of the system.

4.6 0-1 test for chaos

The 0-1 test for chaos, invented by Gottwald and Melbourne [8], is one of the methods for distinguishing between regular and chaotic dynamics of a deterministic system. In contrast to

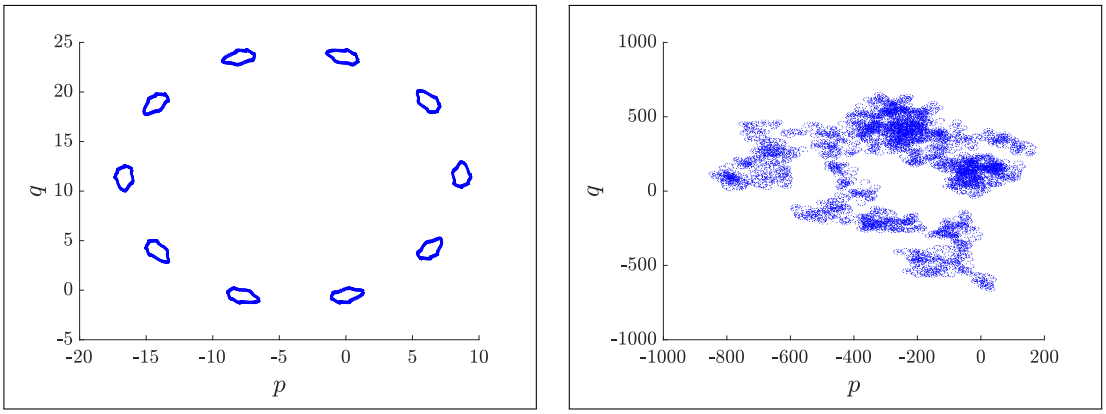

Figure 6: The plot of p versus q for $a = 0.1$ showing regular dynamics (left) and chaotic dynamics for $a = 0.3$ (right) of the Rössler system (15).

the other approaches, the nature of the system is irrelevant, thus the test can be applied directly onto experimental data, ordinary differential equations, or partial differential equations. The results return values close to either 0 or 1, with 0 corresponding to regular dynamics and 1 to chaotic dynamics. With its easy implementation, evaluation, and wide range of application, using this tool for detecting chaos is becoming more popular in different fields. The most recent publications include an alternative test in [32] for noisy data based on the 0-1 test for chaos; improvement of the test evaluation in [21] reducing its computational complexity; investigation of dynamics of a biological model [13] or a model of an electronic circuit [20].

As the 0-1 test was the main topic of my bachelor thesis [26], more details can be found there.

The 0-1 test for chaos can be computed by the following algorithm [8].

Given the observation $\phi(j)$ for $j = 1, 2, ..., N$ and a suitable choice of $c \in (0, 2\pi)$, the following translation variables are computed:

$$p_c(n) = \sum_{j=1}^{n} \phi(j) \cos(jc),$$

$$q_c(n) = \sum_{j=1}^{n} \phi(j) \sin(jc)$$

for $n = 1, 2, ..., N$.

The variables p_c and q_c are bounded if the movement is regular and unbounded, like a Brownian motion, for chaotic dynamics. The difference of a bounded and unbounded trajectory in the (p, q)-plane is in Figure 6 for two values of the parameter a of the Rössler system (15).

The idea for the 0-1 test, first described in [8], is that the boundedness or unboundedness of the trajectory $\{(p_j, q_j)_{j\in[1,N]}\}$ can be studied through the asymptotic growth rate of its time-

averaged mean square displacement (MSD), which is defined as

$$M(n) = \lim_{N\to\infty} \frac{1}{N} \sum_{j=1}^{N} d(j,n)^2$$

where

$$d(j,n) = \sqrt{(p_{j+n} - p_j)^2 + (q_{j+n} - q_j)^2}$$

is the time lapse of the duration n ($n \ll N$) starting from the position at time j. As it is shown in [8, 9], it is important to use values of n small enough compared to N, noted $n_{cut}, (n \leq n_{cut})$. A subset of time lags $n_{cut} \in [1, N/10]$ is advised for the computation of each K_c.

For bounded trajectories and regular dynamics, $M(n)$ is a bounded function in time, whereas unbounded trajectories, meaning chaotic dynamics, are described by $M(n)$ growing linearly with time. Thus the asymptotic growth rate of the MSD must be calculated, which correlates with the unboundedness of the trajectory.

As proposed in [8], the modified MSD is calculated as

$$D(n) = M(n) - E(\phi)^2 \frac{1 - \cos(nc)}{1 - \cos c}$$

The output of the 0-1 test for chaos is computed by the correlation method as

$$K_c = \mathrm{corr}(\xi, \Delta) \in [-1, 1]$$

for the vectors $\xi = (1, 2, ..., n_{cut})$ and $\Delta = (D_c(1), D_c(2), ..., D_c(n_{cut}))$.

The final result of the test is

$$K = \mathrm{median}(K_c).$$

The results of the 0-1 test for chaos K for the range of parameter $a = 0.1$ to $a = 0.3$ of the Rössler system (15) is shown in Figure 7. Values of K close to 0 correspond to the periodic movement visible on the bifurcation diagram (Figure 4), while values close to 1 correspond to chaotic regions. There are also few values of the parameter a, for which K are neither close to 0 nor 1. For these parameters, the 0-1 test failed to identified the dynamics of the system.

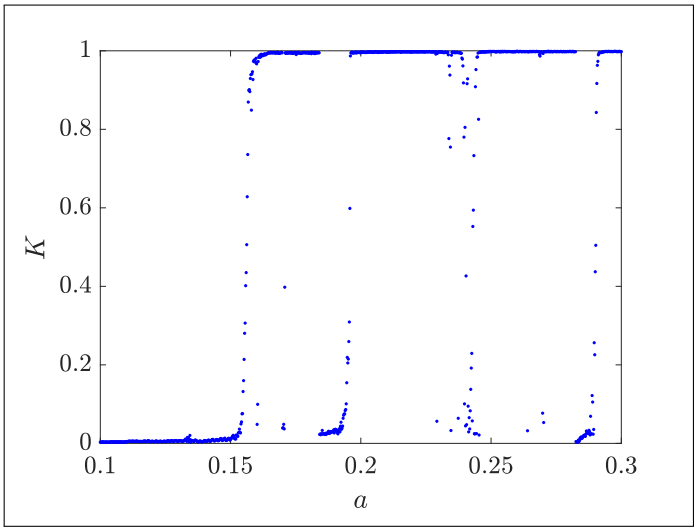

Figure 7: The results of the 0-1 test for chaos K for the range of parameter $a = 0.1$ to $a = 0.3$ of the Rössler system (15).

5 Main results

The results of this study were submitted to Journal of Mathematical Chemistry. The system of ordinary differential equations (14) was solved numerically in Matlab [33] using the *ode*45 solver. The simulations were done depending on free parameter k_f ranging from 3×10^{-4} to 5×10^{-4} with 10^{-7} step. Each simulation was performed for the final time $\tau = 100$ with a time step 10^{-4}. To avoid the systems distortions, only the last 20% of simulations were used for further computations. In all cases, initial conditions were set

$$x_0 = z_0 = v_0 = 1.$$

As a main results, phase diagrams, amplitude frequency spectrums (FFT), and Poincaré sections were done for relevant choices of the parameter k_f. To illustrate changes in dynamical behavior, bifurcation diagrams underlined by the approximate entropy and the 0-1 test for chaos with suitable magnifications to the parameter k_f were plotted.

Consequently, as a goal of this paper, bifurcation diagrams, the approximate entropy, and the 0-1 test for chaos were computed for nested set of parameters k_f. The 0-1 test for chaos splits the values of the parameter for which regular (periodic or quasi-periodic) and irregular (chaotic) movements appear, while the output of approximate entropy detects increasing complexity of the investigated system (14).

5.1 Phase diagrams, the Fourier spectra, and bifurcation diagrams

Periodic as well as chaotic dynamics was identified in the studied model ((14)). For example, in Figure 8 and Figure 9, regular movement is shown by a trivial loop (Figure 8) for $k_f = 3 \times 10^{-4}$, and a non-trivial loop (Figure 9) for $k_f = 3.2 \times 10^{-4}$. Figure 10 gives an example of a chaotic trajectory, that is for $k_f = 3.5 \times 10^{-4}$.

The Fourier spectra were computed by Fast Fourier transform for $k_f = 3 \times 10^{-4}$, $k_f = 3.2 \times 10^{-4}$, and $k_f = 3.5 \times 10^{-4}$, shown in Figs. 8, 9, and 10 respectively. Regular behavior is observable for the first two and chaos in the last case.

In the case of regular movement, in Figure 8 and Figure 9, the Fourier spectra is formed by a number of harmonic frequencies, hence the frequency of the periodic trajectory is computable. Periodic motions of trajectory is also visible in Poincaré sections.

In the case of chaotic movement, Figure 10, the Fourier spectra is formed by a number of harmonic components having the basic, super-harmonic, sub-harmonic, and combination frequencies on which further motions with frequencies forming the sided bands of the dominant frequencies are superposed. Their mutual ratio indicates the irregularity of the motion. The character of this chaotic motion is underlined by the Poincaré section.

Next, the bifurcation diagram (constructed as a projection of a local maxima) of the model (14) was plotted for each variable x, z and v with respect to the free parameter $k_f \in (3 \times 10^{-4}, 5 \times$

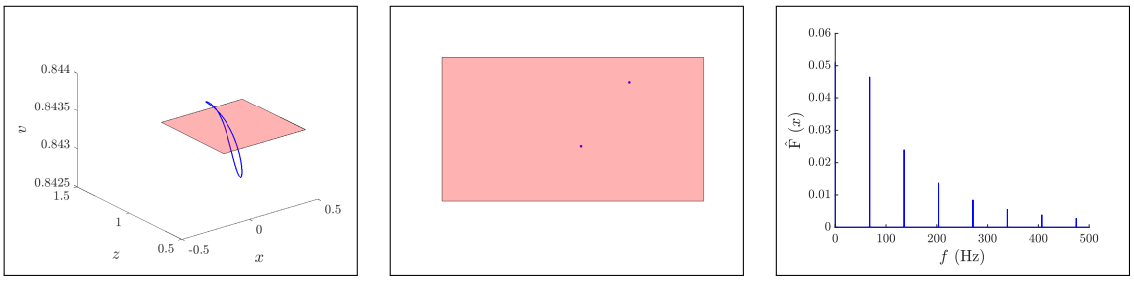

Figure 8: Phase diagram with Poincaré section by plane $v = 0.8434$ and Fourier transform of variable x for $k_f = 3 \times 10^{-4}$.

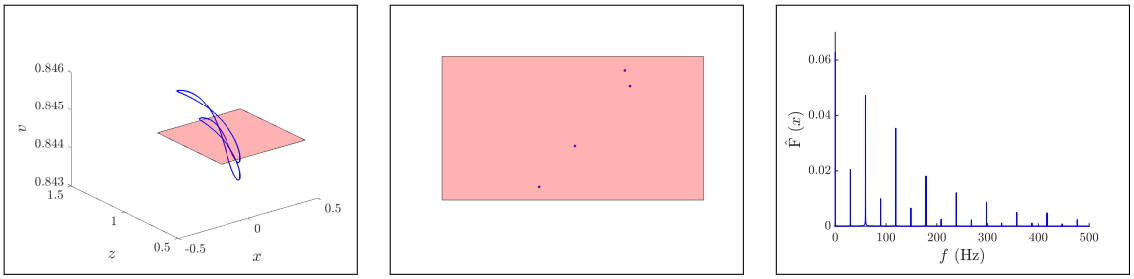

Figure 9: Phase diagram with Poincaré section by plane $v = 0.8445$ and Fourier transform of variable x for $k_f = 3.2 \times 10^{-4}$.

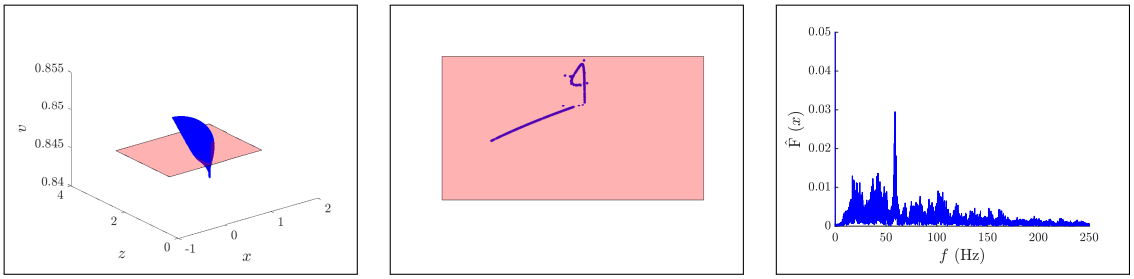

Figure 10: Phase diagram with Poincaré section by plane $v = 0.847$ and Fourier transform of variable x for $k_f = 3.5 \times 10^{-4}$.

10^{-4}) in Figure 11. In this bifurcation diagram, so-called "period doubling" and "windows" effects are also visible. Periodic movement can be identified in the range of the parameter, e.g., $k_f \in (3 \times 10^{-4}, 3.24 \times 10^{-4})$ and $k_f \in (3.95 \times 10^{-4}, 5 \times 10^{-4})$. The interval in between these values is interrupted by chaotic cases around $k_f = 3.25$, and some $k_f \in (3.34 \times 10^{-4}, 3.65 \times 10^{-4})$ and $k_f \in (3.85 \times 10^{-4}, 3.9 \times 10^{-4})$.

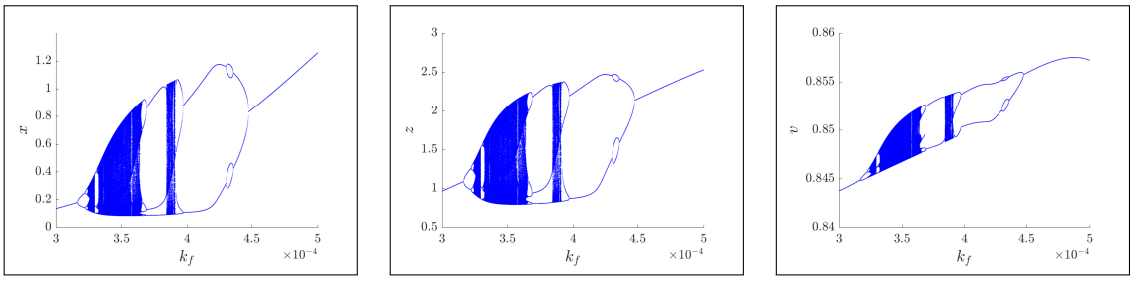

Figure 11: Bifurcation diagram of the variable x(left), z(center), v(right) $k_f \in [3 \times 10^{-4}, 5 \times 10^{-4}]$.

5.2 Approximate entropy

The approximate entropy was calculated using the *TSEntropies* package [36] for R [31]. The computations were made for the input vector s given in a normalized form of all state variables:

$$s(t) = \sqrt{x^2(t) + z^2(t) + v^2(t)},$$

$k_f \in (3 \times 10^{-4}, 5 \times 10^{-4})$ and $r = 0.1$. The results of approximate entropy for all values of the parameter k_f are in Figs. 14–16

5.3 0-1 test for chaos

For these simulations, a free software environment R [31] was used including the *Chaos01* package developed by T. Martinovič [22]. The position of the studied system ((14)) at any moment of time is determined by displacements x, z, and v, which are used for defining vector ϕ:

$$\phi(j) = \sqrt{x(j)^2 + z(j)^2 + v(j)^2}.$$

The dynamics of the translation components p_c and q_c is shown on the p_c versus q_c plot. An example of a bounded trajectory is in Figure 12 on the left, and an unbounded trajectory on the right.

Comparison of values K_c for periodic and chaotic case is shown in Figure 13, for $k_f = 3 \times 10^{-4}$ and $k_f = 3.5 \times 10^{-4}$, respectively.

The results of the 0-1 test for chaos for all values of the parameter k_f are in Figs. 14–16.

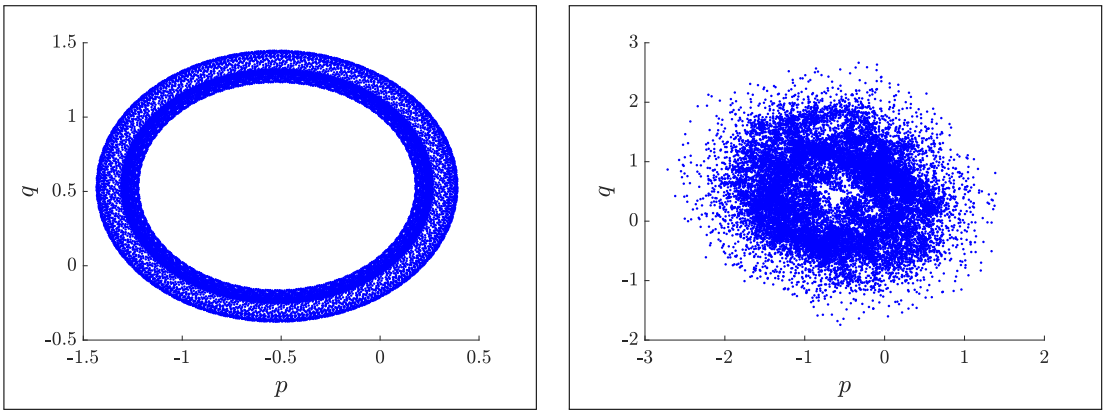

Figure 12: The plot of p versus q for $c = 1.569853$ for $k_f = 3 \times 10^{-4}$ showing regular dynamics (left) and chaotic dynamics for $k_f = 3.5 \times 10^{-4}$(right).

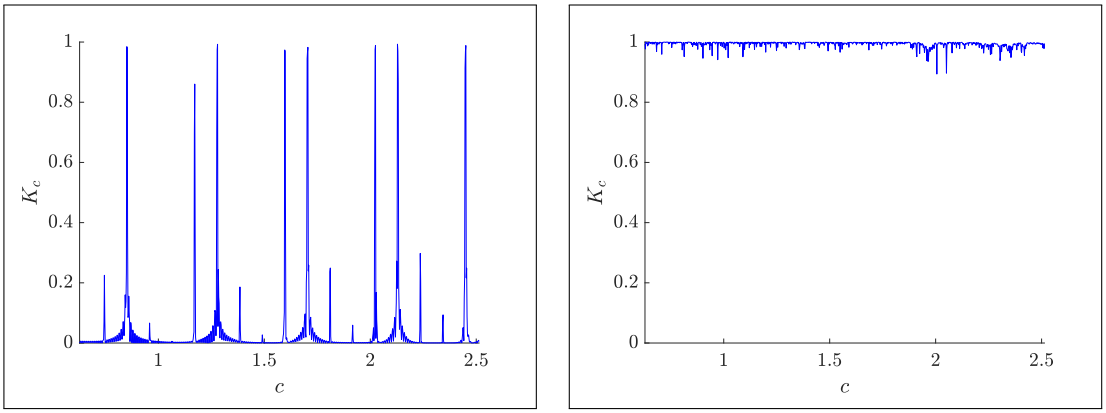

Figure 13: The plot of K_c based on c for $k_f = 3 \times 10^{-4}$ showing regular dynamics (left) and for $k_f = 3.5 \times 10^{-4}$ showing chaotic dynamics (right).

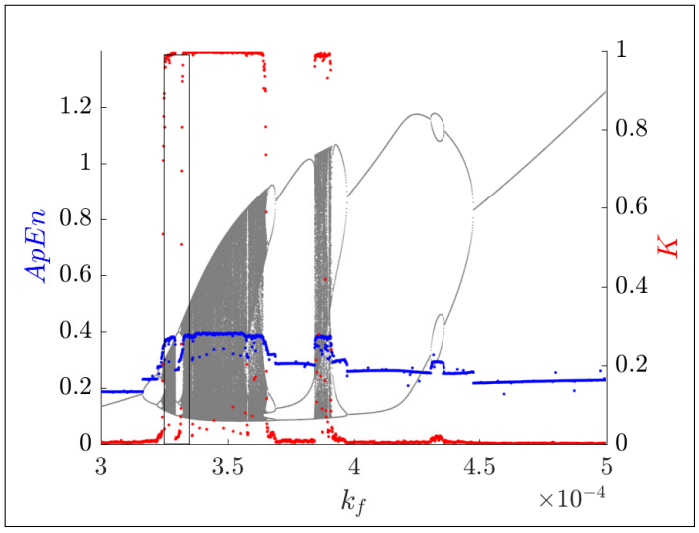

Figure 14: The result of approximate entropy (in blue) and the result of the 0-1 test for chaos (in red) for $k_f \in (3 \times 10^{-4}, 5 \times 10^{-4})$. The magnification in the black rectangle is shown in Fig 15. The bifurcation diagram for variable x is shown in the background.

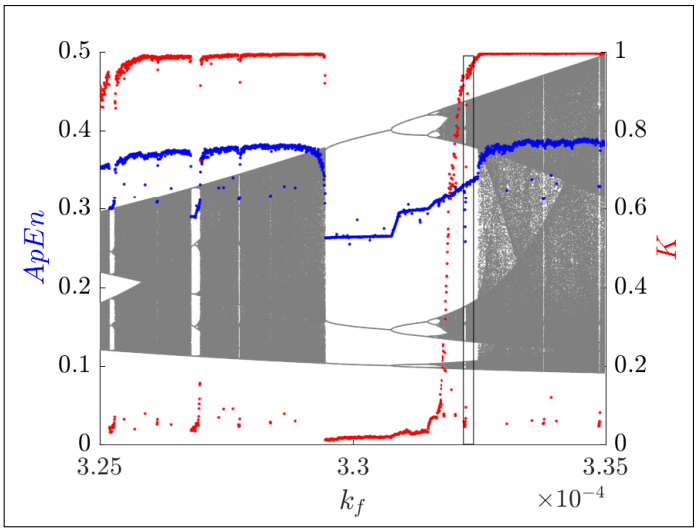

Figure 15: The result of approximate entropy (in blue) and the result of the 0-1 test for chaos (in red) for $k_f \in (3.25 \times 10^{-4}, 3.35 \times 10^{-4})$. The magnification in the black rectangle is shown in Fig 16. The bifurcation diagram for variable x is shown in the background.

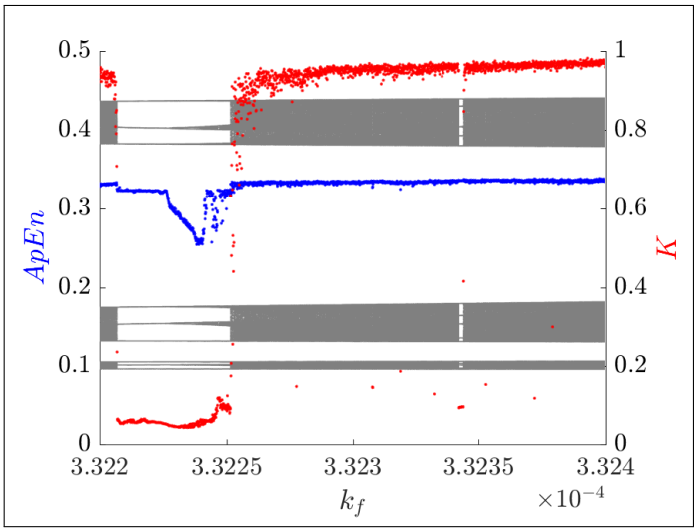

Figure 16: The result of approximate entropy (in blue) and the result of the 0-1 test for chaos (in red) for $k_f \in (3.322 \times 10^{-4}, 3.324 \times 10^{-4})$. The bifurcation diagram for variable x is shown in the background.

6 Matlab source codes

This section presents the implementation of the BZ reaction (14) as well as the tools for dynamics detection, such as the phase portraits, Poincaré sections, and Fast Fourier transform.

6.1 Implementation of the model

The code 1 listed below sets up the interval of the parameter k_f, $k_f \in [a, b]$, as well as the initial conditions and time span. The *ode45* solver calls the function `Func3` listed in 2.

```
parpool(cluster,24)

a=3/10000; %interval
b=5/10000;
step=0.001/10000;

parfor kff=1:1:2001
kf=kff*step+a-step;

x0 = 1;
z0 = 1;
w0 = 1;

v0 = [x0,z0,w0]; %initial conditions

tspan = 0:0.0001:100; %time span

options = odeset('RelTol',1.e-10,'AbsTol',1.e-10);
[t,v] = ode45(@(t,v)Func3(t,v,kf),tspan,v0,options);

filename=[ 'BZ3_kff=' num2str(kff) '.mat'];
parsave(filename,t,v,kf);
end

parpool close;
quit
```

Listing 1: Code for solving the set of differential equations (14).

```
function ddt=Func3(t,v,kf)
 x = v(1);
```

```
z = v(2);
w = v(3);

k1 = 4*10^6;
k2 = 2;
k3 = 3000;
k4 = 55.2;
k5 = 7000;
k6 = 0.09;
k7 = 0.23;

A = 0.1; %[BrO3-]
M = 0.25; %[MA]
H = 0.26; %[H+]
C = 0.000833; %[Ce]
a = 666.7;
b = 0.3478;

T0 = (10*k2*A*H*C)^-1;
X0 = k2*A*H^2/k5;
Y0 = 4*k2*A*H^2/k5;
Z0 = C*A/(40*M);
V0 = 4*A*H*C/M^2;

yy = (a*k6*Z0*V0*z*w/(k1*H*X0*x+k2*A*H^2+kf))/Y0;

dxdt = T0*(-k1*H*Y0*x*yy + k2*A*H^2*Y0*X0^-1*yy - 2*k3*X0*x^2 + (1/2)*k4*A
    ^(1/2)*H^(3/2)*X0^(-1/2)*(C-Z0*z)*x^(1/2) - (1/2)*k5*Z0*x*z - kf*x);
dzdt = T0*(k4*A^(1/2)*H^(3/2)*X0^(1/2)*(C/Z0-z)*x^(1/2) - k5*X0*x*z - a*k6*V0*
    z*w - b*k7*M*z - kf*z);
dwdt = T0*(2*k1*H*X0*Y0*V0^(-1)*x*yy + k2*A*H^2*Y0*V0^-1*yy + k3*X0^2*V0^-1*x
    ^2 - a*k6*Z0*z*w - kf*w);
ddt = [dxdt; dzdt; dwdt];
end
```

Listing 2: Implementation of (14), `Func3` called by 1.

6.2 Codes for tools of dynamics detection

In Section 4, methods for dynamics detection were introduced, such as phase portraits, Poincaré sections, Fast Fourier transform, and bifurcation diagrams.

The Matlab code for plotting the 3D phase portrait 3 shows that we plot the last 20% of the trajectory, in order to avoid the initial phase and reach the system's attractor.

```
plot3(v(800000:end,1),v(800000:end,2),v(800000:end,3),'b');
ax = gca;
ax.FontSize = 16;
ax.TickLabelInterpreter = 'latex';
xlabel('\(x\)','fontsize',20,'interpreter','latex');
ylabel('\(z\)','fontsize',20,'interpreter','latex');
zlabel('\(v\)','fontsize',20,'interpreter','latex');
```

Listing 3: Matlab code for 3D phase portraits drawing the system's attractor consisting of a 3-dimensional vector v.

The code for the Poincaré sections 4 shows the construction of the plane, then finding the intersection points, and plotting two figrues. The first shows the trajectory of the system with the plane intersecting it. The points of intersection on the plane are shown on the second figure.

```
load('BZ3_kff=501.mat')

data_u = v(1:end,1);
data_v = v(1:end,2);
data_w = v(1:end,3);

% define plane
vec_u = [1 0 0];
vec_u = vec_u/norm(vec_u);
vec_v = [0 1 0];
vec_v = vec_v/norm(vec_v);

A = [0.1 0.8 0.8445];
t = [-0.25 0.35];
s = [-0.25 0.35];

% plot phase portrait
x = [A(1)+min(t)*vec_u(1)+min(s)*vec_v(1), A(1)+max(t)*vec_u(1)+min(s)*vec_v(1)
    , A(1)+max(t)*vec_u(1)+max(s)*vec_v(1), A(1)+min(t)*vec_u(1)+max(s)*vec_v
    (1)];
```

```
y = [A(2)+min(t)*vec_u(2)+min(s)*vec_v(2), A(2)+max(t)*vec_u(2)+min(s)*vec_v(2)
    , A(2)+max(t)*vec_u(2)+max(s)*vec_v(2), A(2)+min(t)*vec_u(2)+max(s)*vec_v
    (2)];
z = [A(3)+min(t)*vec_u(3)+min(s)*vec_v(3), A(3)+max(t)*vec_u(3)+min(s)*vec_v(3)
    , A(3)+max(t)*vec_u(3)+max(s)*vec_v(3), A(3)+min(t)*vec_u(3)+max(s)*vec_v
    (3)];
figure();
plot3(data_u(800001:1:end),data_v(800001:1:end),data_w(800001:1:end),'b','
    LineWidth',1.5);
ax = gca;
ax.FontSize = 16;
ax.TickLabelInterpreter = 'latex';
xlabel('\(x\)','fontsize',20,'interpreter','latex');
ylabel('\(z\)','fontsize',20,'interpreter','latex');
zlabel('\(v\)','fontsize',20,'interpreter','latex');
patch(x,y,z,'red','FaceAlpha',.3)

intrs = [];
prec = 10^(-4);
for a = 800000:1:1000001
    s1 = (data_v(a)-A(2)-((data_u(a)*vec_u(2))/vec_u(1))-((A(1)*vec_u(2))/vec_u
        (1)))/(vec_v(2)-(vec_v(1)*vec_u(2))/vec_u(1));
    t1 = (data_u(a)-A(1)-s1*vec_v(1))/vec_u(1);
    z1 = A(3)+t1*vec_u(3)+s1*vec_v(3);
    if data_w(a)>=(z1-prec) && data_w(a)<=(z1+prec) && s1>=min(s) && s1<=max(s)
         && t1>=min(t) && t1<=max(t)
        intrs = [intrs a];
    end
end

start = intrs(1);
interp_x = [];
interp_y = [];
interp_z = [];

for a = 2:length(intrs)
    if (intrs(a)-intrs(a-1)) > 1
        if a == length(intrs)
            stop = intrs(end);
```

```
        else
            stop = intrs(a-1);
        end

        if stop - start > 1
        vector_u = (data_u(start)+data_u(stop))/2;
        vector_v = (data_v(start)+data_v(stop))/2;

        s11 = (vector_v-A(2)-((vector_u*vec_u(2))/vec_u(1))-((A(1)*vec_u(2))/
            vec_u(1)))/(vec_v(2)-(vec_v(1)*vec_u(2))/vec_u(1));
        t11 = (vector_u-A(1)-s11*vec_v(1))/vec_u(1);
        value = A(3)+t11*vec_u(3)+s11*vec_v(3);
        interp_z = [interp_z, value];

        dataIndex = spline(data_w(start:stop),start:stop,value);
        interp_x = [interp_x, spline(start:stop,data_u(start:stop),dataIndex)];
        interp_y = [interp_y, spline(start:stop,data_v(start:stop),dataIndex)];
        end

        start = intrs(a);
    end
end

figure();
plot3(interp_x,interp_y,interp_z,'.b','MarkerSize',10);
patch(x,y,z,'red','FaceAlpha',.3)
axis([min(x) max(x) min(y) max(y)])
view(-180, 66.32)
ax = gca;
ax.Visible = 'off';
```

Listing 4: Matlab code for Poincaré sections.

The Fast Fourier transform is computed and plotted using the following code 5.

```
T = 0.0001;
Fs = 1/T;
load('BZ3_kff=501.mat')

X = v(800000:end,1)';
L = length(X);
```

```
Y = fft(X);

P2 = abs(Y/L);
P1 = P2(1:L/2+1);
P1(2:end-1) = 2*P1(2:end-1);

f = Fs*(0:(L/2))/L;

FK_fft = [f;P1];


fmax = 250; ymax = 0.05;

f = FK_fft(1,:);
f = f(f<fmax);
frqLength = numel(f);
P1 = FK_fft(2,1:frqLength);

plot(f,P1,'Color','b','LineWidth',1)
xlabel('\(f\) (Hz)')
ylabel('\^{F} \((x)\)')
xlim([0 fmax]); ylim([0 ymax]);
ax = gca;
ax.FontSize = 16;
ax.TickLabelInterpreter = 'latex';
xlabel('\(f\) (Hz)','fontsize',20,'interpreter','latex');
ylabel('\^{F} \((x)\)','fontsize',20,'interpreter','latex');
box off
```

Listing 5: Matlab code for computing the Fast Fourier transform and plotting the frequency spectrum.

The bifurcation diagram was done by plotting the maxima of the trajectory for each value of the parameter k_f. First, the maxima are found and stored in a matrix using the code 6. The bifurcation diagram is then plotted from the matrix by 7.

```
M=zeros(100000,2001);

for a = 1:1:2001
   nameRes = [ 'BZ3_kff=',num2str(a),'.mat' ];
   data = load(nameRes);
```

```
    X = data.v(900002:1000001,1);

    for i=1:length(X)
         M(i,a) = X(i);
    end;
end


N = M';

[npar,nite] = size(N);
T = zeros(npar,nite);
T2 = zeros(npar,nite);
NT = zeros(npar,nite);

for i = 1:npar
    for j = 2:nite-1
        if(N(i,j)>=N(i,j-1) && N(i,j)>=N(i,j+1)) %maximum
            T(i,j) = 1;
        else
            T(i,j) = 0;
        end
    end
end

NT = T.*N;
NT = round(NT,10);

for i = 1:npar
    [~, k, ~] = unique(NT(i,:),'stable');
    T2(i,k) = 1;
end

NTT = T2.*NT;
NTT(NTT == 0) = NaN;

save('bif_BZ3_x','NTT','-v7.3');
```

Listing 6: Matlab code for searching for the maxima of variable x for each parameter to plot it in a bifurcation diagram.

```
function bif_diagram(XX)
tic
[row,col]=size(XX);
a = 3/10000;
b = 5/10000;
r_ = linspace(a,b,row);

for k = 1:col
    plot(r_,XX(:,k),'.','Color',[0.5 0.5 0.5],'MarkerSize',.2); hold on
end
xlabel('\(k_f\)','fontsize',20,'interpreter','latex');
ylabel('\(x\)','fontsize',20,'interpreter','latex');
ax = gca;
ax.FontSize = 16;
ax.TickLabelInterpreter = 'latex';
xlim([a b])
toc
end
```

Listing 7: Matlab code for plotting the matrix obtained by 6 resulting in the bifurcation diagram.

7 Conclusions

In this thesis, the GF model (14) associated with the BZ chemical reaction was extensively researched by massive simulation and graphical analysis. The corresponding system of ordinary differential equations (14) was implemented in Matlab [33]. In order to solve the system, the adaptive six-stage, fifth-order, Runge-Kutta method implemented as *ode*45 solver, was used.

The simulations were used to plot 3D phase portraits, bifurcation diagrams, approximate entropy, and the 0-1 test for chaos. The mining process of dynamical properties were performed in the free software R [31] using packages *TSEntopies* [36] and *Chaos*01 [22] depending on flow rate parameter k_f.

It is evident from main results in Figs. 14–16 that both tests detect regular and irregular patterns for given k_f. Our results show that the method of approximate entropy returns quantification constant which describes complexity in the system invariantly with respect to the origin. On the other hand, the 0-1 test as qualification tool returns values close to 0 for regular (periodic or quasi-periodic) movement and values close to 1 for irregular (chaos) characteristics.

Further, we observe a correlation between approximate entropy and the 0-1 test for chaos. In general, values of the 0-1 test for chaos $K \approx 0$ are paired with low values of approximate entropy and analogously, results $K \approx 1$ are related to high values of approximate entropy. More precisely, one can find a minimal value E_0 of approximate entropy for which the corresponding 0-1 test for chaos returns $K \approx 1$. Therefore E_0 is a critical value of the approximate entropy for which for all the values E_1, $E_1 < E_0$, the 0-1 test returns $K \approx 0$, and for E_2, $E_2 > E_0$, the system's complexity corresponds to $K \approx 1$. For $k_f \in (3 \times 10^{-4}, 5 \times 10^{-4})$ on Figure 14, the critical value is estimated as $E_0 \approx 0.36$.

We notice isolated values of the 0-1 test for chaos $K \approx 0$ accompanied by comparatively low values of approximate entropy well within the chaotic region characterized by high values of approximate entropy and high values of the 0-1 test, $K \approx 1$. To investigate and zoom in, we have constructed a three-stage system of nested subintervals of flow rates k_f, see Figs. 14–16, for which in every level the 0-1 test for chaos and approximate entropy was computed. At every level we observe the same pattern. That naturally yields suggestion of a fractal structure in the set of k_f:

Open Problem 1 *Is there a totally disconnected (Cantor) set of flow rates k_f in $[3 \times 10^{-4}, 5 \times 10^{-4}]$ such that for each such parameter the GF model* (14) *is showing chaos?*

Open Problem 2 *Is there a totally disconnected (Cantor) set of flow rates k_f in $[3 \times 10^{-4}, 5 \times 10^{-4}]$ such that for each such parameter the GF model* (14) *is showing regular movement?*

This hypothesis will be addressed in future work by constructing more nested subintervals using high precision computing.

References

[1] ADAMATZKY, Andrew, Benjamin DE LACY COSTELLO, Peter DITTRICH, Jerzy GORECKI and Klaus-Peter ZAUNER. On logical universality of Belousov-Zhabotinsky vesicles. *International Journal of General Systems*. 2014, **43**(7), 757-769. ISSN 0308-1079.

[2] ALFIFI, H. Y., T. R. MARCHANT and M. I. NELSON. Non-smooth feedback control for Belousov–Zhabotinskii reaction–diffusion equations: semi-analytical solutions. *Journal of Mathematical Chemistry*. 2016, **54**(8), 1632-1657. ISSN 0259-9791.

[3] AZHAND, Arash, Rico BUCHHOLZ, Jan F. TOTZ and Harald ENGEL. A novel technique to initiate and investigate scroll waves in thin layers of the photosensitive Belousov-Zhabotinsky reaction. *The European Physical Journal E*. 2016, **39**(6). ISSN 1292-8941.

[4] BAIER, G., K. WEGMANN and J.L. HUDSON. An intermittent type of chaos in the Belousov-Zhabotinsky reaction. *Physics Letters A*. 1989, **141**(7), 340-345. ISSN 0375-9601.

[5] BERLANGA, Isadora. Synthesis of Non-Uniform Functionalized Amphiphilic Block Copolymers and Giant Vesicles in the Presence of the Belousov–Zhabotinsky Reaction. *Biomolecules*. 2019, **9**(8), 352. ISSN 2218-273X.

[6] BUDRONI, M. A., M. RUSTICI and E. TIEZZI. On the Origin of Chaos in the Belousov-Zhabotinsky Reaction in Closed and Unstirred Reactors. *Mathematical Modelling of Natural Phenomena*. 2011, **6**(1), 226-242. ISSN 0973-5348.

[7] FIELD, Richard J. Chaos in the Belousov–Zhabotinsky reaction. *Modern Physics Letters B*. 2015, **29**(34). ISSN 0217-9849.

[8] GOTTWALD, Georg A. and Ian MELBOURNE. On the Implementation of the 0–1 Test for Chaos. *SIAM Journal on Applied Dynamical Systems*. 2009, **8**(1), 129-145. ISSN 1536-0040.

[9] GOTTWALD, Georg A. and Ian MELBOURNE. On the validity of the 0–1 test for chaos. *Nonlinearity*. 2009, **22**(6), 1367-1382. ISSN 0951-7715.

[10] GYÖRGYI, László and Richard J. FIELD. A three-variable model of deterministic chaos in the Belousov–Zhabotinsky reaction. *Nature*. 1992, **355**(6363), 808-810. ISSN 0028-0836.

[11] GYÖRGYI, László and Richard J. FIELD. Simple models of deterministic chaos in the Belousov-Zhabotinskii reaction. *The Journal of Physical Chemistry*. 1991, **95**(17), 6594-6602. ISSN 0022-3654.

[12] GYÖRGYI, László, Susan L. REMPE and Richard J. FIELD. A novel model for the simulation of chaos in low-flow-rate CSTR experiments with the Belousov-Zhabotinskii reaction: a chemical mechanism for two-frequency oscillations. *The Journal of Physical Chemistry*. 1991, **95**(8), 3159-3165. ISSN 0022-3654.

[13] HALFAR, Radek. Dynamical properties of Beeler–Reuter cardiac cell model with respect to stimulation parameters. *International Journal of Computer Mathematics*. 2020, **97**(1-2), 498-507. ISSN 0020-7160.

[14] HALFAR, Radek. Characterization of Cardiac Cell Electrophysiology Model Using Recurrence Plots. In: *Chaos and Complex Systems*. STAVRINIDES, Stavros G. and Mehmet OZER, ed. Springer International Publishing, 2020, s. 73-81. ISBN 978-3-030-35440-4.

[15] HARA, Yusuke and Yoshiko TAKENAKA. Autonomous Oscillation of Polymer Chains Induced by the Belousov–Zhabotinsky Reaction. *Sensors*. 2014, **14**(1), 1497-1510. ISSN 1424-8220.

[16] HOU, Jingyu, Xianghong LI and Jufeng CHEN. Stability and slow-fast oscillation in fractional-order Belousov-Zhabotinsky reaction with two time scales. *Journal of Vibroengineering*. 2016, **18**(7), 4812-4823. ISSN 1392-8716.

[17] JUN, Wang, Tang LINGYU, Zhang XIANYONG and Luo YUYAN. Three-way weighted combination-entropies based on three-layer granular structures. *Applied Mathematics and Nonlinear Sciences*. 2017, **2**(2), 329-340. ISSN 2444-8656.

[18] KISS, I. Electric field effects on travelling waves in the Oregonator model for the Belousov-Zhabotinsky reaction. *The Quarterly Journal of Mechanics and Applied Mathematics*. 2004, **57**(4), 467-494. ISSN 0033-5614.

[19] KOLAR-ANIC, Ljiljana, Slavica BLAGOJEVIC, Natasa PEJIC, Nebojsa BEGOVIC, Stevan BLAGOJEVIC and Slobodan ANIC. New evidence of transient complex oscillations in a closed, well-stirred Belousov-Zhabotinsky system. *Journal of the Serbian Chemical Society*. 2006, **71**(6), 605-612. ISSN 0352-5139.

[20] LAMPART, Marek and Judita NAGYOVÁ. Movement Characteristics of a Model with Circular Equilibrium. In: *Chaos and Complex Systems*. STAVRINIDES, Stavros G. and Mehmet OZER, ed. Springer International Publishing, 2020, s. 45-55. ISBN 978-3-030-35440-4.

[21] MARTINOVIČ, Tomáš. Alternative approaches of evaluating the 0–1 test for chaos. *International Journal of Computer Mathematics*. 2020, **97**(1-2), 508-521. ISSN 0020-7160.

[22] MARTINOVIČ, Tomáš. *Chaos01: 0-1 Test for Chaos* [software]. 2019. Available from: `https://CRAN.R-project.org/package=Chaos01`.

[23] MERKIN, J. H. Travelling waves in the Oregonator model for the BZ reaction. *IMA Journal of Applied Mathematics*. 2009, **74**(4), 622-643. ISSN 0272-4960.

[24] MERKIN, J. H. On wave trains arising in the two-variable Oregonator model for the BZ reaction. *IMA Journal of Applied Mathematics*. 2013, **78**(3), 513-536. ISSN 0272-4960.

[25] MYINT, Aung Zaw, Li LI and Ming Xin WANG. Qualitative analysis of a Belousov–Zhabotinskii reaction model. *Acta Mathematica Sinica, English Series*. 2018, **34**(6), 975-991. ISSN 1439-8516.

[26] NAGYOVÁ, Judita. *"0-1" test for chaos*. Ostrava, 2018. Diplomová práce. Vysoká škola báňská - Technická univerzita Ostrava.

[27] NAGYOVÁ, Judita, Branislav Jansík and Marek LAMPART. Revised dynamics of the Belousov-Zhabotinsky reaction model [preprint]. 2020. Available from: `https://arxiv.org/abs/2005.03325`.

[28] PINCUS, S. M. Approximate entropy as a measure of system complexity. *Proceedings of the National Academy of Sciences*. 1991, **88**(6), 2297-2301. ISSN 0027-8424.

[29] RÖSSLER, O.E. An equation for continuous chaos. *Physics Letters A*. 1976, **57**(5), 397-398. ISSN 0375-9601.

[30] PRIGOGINE, I. and R. LEFEVER. Symmetry Breaking Instabilities in Dissipative Systems. II. *The Journal of Chemical Physics*. 1968, **48**(4), 1695-1700. ISSN 0021-9606

[31] R CORE TEAM. *R: A Language and Environment for Statistical Computing* [software]. 2018. Available from: `https://www.R-project.org/`.

[32] TEMPELMAN, Joshua R. and Firas A. KHASAWNEH. A look into chaos detection through topological data analysis. *Physica D: Nonlinear Phenomena*. 2020, **406**. ISSN 0167-2789.

[33] THE MATHWORKS INC. MATLAB *R2015b* [software]. 2015. Available from: `https://www.mathworks.com/`.

[34] TLIDI, Mustapha, Yerali GANDICA, Giorgio SONNINO, Etienne AVERLANT and Krassimir PANAJOTOV. Self-Replicating Spots in the Brusselator Model and Extreme Events in the One-Dimensional Case with Delay. *Entropy*. 2016, **18**(3). ISSN 1099-4300.

[35] TOMČALA, Jiří. Acceleration of time series entropy algorithms. *The Journal of Supercomputing*. 2019, **75**(3), 1443-1454. ISSN 0920-8542.

[36] TOMČALA, Jiří. *TSEntropies: Time Series Entropies* [software]. 2018. Available from: `https://CRAN.R-project.org/package=TSEntropies`.

[37] TOMITA, Kazuhisa and Ichiro TSUDA. Chaos in the Belousov-Zhabotinsky reaction in a flow system. *Physics Letters A*. 1979, **71**(5-6), 489-492. ISSN 0375-9601.

[38] TURING, A. M. The chemical basis of morphogenesis. *Philosophical Transactions of the Royal Society of London, Series B*. 1997, **237**(641), 37-72. ISSN 2054-0280

[39] TYSON, John J. What Everyone Should Know About the Belousov-Zhabotinsky Reaction. In: *Lecture Notes in Biomathematics*. LEVIN, Simon A., ed. Springer Berlin Heidelberg, 1994, s. 569-587. ISBN 978-3-642-50126-5.

[40] ZHOU, Jun. Bifurcation analysis of the Oregonator model. *Applied Mathematics Letters*. 2016, **52**, 192-198. ISSN 08939659.

[41] ZHYROVA, Anna and Dalibor ŠTYS. Construction of the phenomenological model of Belousov–Zhabotinsky reaction state trajectory. *International Journal of Computer Mathematics*. 2014, **91**(1), 4-13. ISSN 0020-7160.

A Appendix

The results were achieved in collaboration with Mgr. Branislav Jansík, Ph.D. and doc. RNDr. Marek Lampart, Ph.D., and were submitted to Journal of Mathematical Chemistry (Jimp-type journal located in Q2). The preprint of the article is available at arXiv.org as [27]. The original article *Revised dynamics of the Belousov-Zhabotinsky reaction model* follows.

Journal of Mathematical Chemistry manuscript No.
(will be inserted by the editor)

Revised dynamics of the Belousov-Zhabotinsky reaction model

Judita Nagyová · Branislav Jansík · Marek Lampart

Received: date / Accepted: date

Abstract The main aim of this paper is to detect dynamical properties of the Györgyi-Field model of the Belousov-Zhabotinsky chemical reaction. The corresponding three-variable model given as a set of nonlinear ordinary differential equations depends on one parameter, the flow rate. As certain values of this parameter can give rise to chaos, the analysis was performed in order to identify different dynamics regimes. Dynamical properties were qualified and quantified using classical and also new techniques. Namely, phase portraits, bifurcation diagrams, the Fourier spectra analysis, the 0-1 test for chaos, and approximate entropy. The correlation between approximate entropy and the 0-1 test for chaos was observed and described in detail. Moreover, the three-stage system of nested subintervals of flow rates, for which in every level the 0-1 test for chaos and approximate entropy was computed, is showing the same pattern. The study leads to an open problem whether the set of flow rate parameters has Cantor like structure.

Keywords Belousov-Zhabotinsky reaction · Györgyi-Field model · 0-1 test for chaos · approximate entropy · bifurcation

Mathematics Subject Classification (2010) 37N99 · 65P20 · 34D08 · 37M25

1 Introduction

The Belousov-Zhabotinsky chemical reaction (BZ reaction), originally discovered in the 1950s by Boris P. Belousov [30], is an example of oscillating chemical reaction which can be maintained far from

Judita Nagyová
IT4Innovations, VŠB - Technical University of Ostrava, 17. listopadu 15/2172, 708 33 Ostrava, Czech Republic
Department of Applied Mathematics, VŠB - Technical University of Ostrava, 17. listopadu 15/2172, 708 33 Ostrava, Czech Republic
E-mail: judita.nagyova.st@vsb.cz

Branislav Jansík
IT4Innovations, VŠB - Technical University of Ostrava, 17. listopadu 15/2172, 708 33 Ostrava, Czech Republic
E-mail: branislav.jansik@vsb.cz

Marek Lampart
IT4Innovations, VŠB - Technical University of Ostrava, 17. listopadu 15/2172, 708 33 Ostrava, Czech Republic
Department of Applied Mathematics, VŠB - Technical University of Ostrava, 17. listopadu 15/2172, 708 33 Ostrava, Czech Republic
E-mail: marek.lampart@vsb.cz

equilibrium by an internal source of energy [2] resulting in a nonlinear chemical oscillator exhibiting different dynamical regimes. Later on, the chemical mechanism of the reaction was described in [4], what is commonly called the FKN mechanism.

There are many mathematical models representing different aspects of the BZ reaction. For example, the Brusselator, Oregonator and Györgyi-Field are three mathematical models for a type of autocatalytic reaction – like the BZ reaction.

The Oregonator model is the result of a quantitative kinetic analysis of oscillations in the BZ reaction by Field and Noyes in 1974 [5] and it is a simplified version of the mechanism developed by Field, Körös and Noyes (FKN mechanism) [30].

The Brusselator model, a theoretical model for a type of autocatalytic reaction, was proposed by I. Prigogine and his collaborators [6].

Finally, the Györgyi-Field model (GF model), describes the reaction taking place in a continuous-flow stirred-tank reactor (CSTR) [10], by a relatively simple mathematical model (see also [11] and [9]). This model, for a specific choice of parameters, exhibits chaos (see e.g. [3] and references therein or main results of this paper), on contrary to the Oregonator which has no chaotic solutions [31] describing the oscillatory behaviour and pattern formation in the BZ reaction. The GF model will be taken into consideration for further research in this paper.

In recent decades, the BZ reaction has been extensively studied by physical chemists on its kinetic behaviour [3,23,29] and by mathematicians on the dynamics and patterns of the solutions of the associated mathematical model [26,20,24,31].

More specifically, the research from the theory of dynamical system point of view was done. The transition from steady state to quasi-periodic and bursting oscillations, and further on to regular relaxation oscillation via a complicated sequence of alternating periodic and chaotic regimes were done by simulations in [19]. The results of computer experiments on information processing in a hexagonal array of vesicles filled with BZ solution in a sub-excitable mode were introduced by [1]. The discretized version of BZ reaction models was also researched. E.g. in [15], the dynamics of the local map is discussed, the set of trajectories that escape to infinity as well as analyze the set of bounded trajectories – the Julia set of the system. The evidence of chaos was also demonstrated in an experimental way by dozens works e.g. [25,32,13].

Despite a large number of results in the given area, it is possible to apply new methods to the given BZ reaction model and to obtain new very interesting results that better characterize the trajectory behaviour depending on the choice of state parameters showing properties of the parameter space.

This work focuses on the characterization of dynamical properties of the GF model [10] depending on the flow rate, denoted by k_f. The qualitative and quantitative characterization of the dynamics regimes is mainly done using the 0-1 test for chaos and approximate entropy. Recall that these tools were applied in [16] to the two-dimensional coupled map lattice model of the Lagrangian type, which is a discrete version of the BZ reaction. These tools were applied to the huge simulation data that was performed on the Salomon supercomputer at IT4Innovations National Supercomputing Center located in Ostrava, Czech Republic.

The paper is organized as follows: in Section 2 the model is introduced, followed by its mathematical model in Section 3. The main results obtained by phase portraits, the Fourier spectra analysis, the approximate entropy, and the 0-1 for chaos, are contained in Section 4. Finally, the outcomes are summarized in Section 5.

Table 1 Rates and rate constants of the GF model chemical scheme.

Reaction equation	Rate r_i	Rate constant k_i
(1a)	$r_1 = k_1 HYX$	$k_1 = 4.0 \times 10^6\, M^{-2} s^{-1}$
(1b)	$r_2 = k_2 AH^2 Y$	$k_2 = 2.0\, M^{-3} s^{-1}$
(1c)	$r_3 = k_3 X^2$	$k_3 = 3000\, M^{-1} s^{-1}$
(1d)	$r_4 = k_4 A^{0.5} H^{1.5} (C - Z) X^{0.5}$	$k_4 = 55.2\, M^{-2.5} s^{-1}$
(1e)	$r_5 = k_5 XZ$	$k_5 = 7000\, M^{-1} s^{-1}$
(1f)	$r_6 = \alpha k_6 ZV$	$k_6 = 0.09\, M^{-1} s^{-1}$
(1g)	$r_7 = \beta k_7 MZ$	$k_7 = 0.23\, M^{-1} s^{-1}$

2 The Györgyi-Field reaction model

The GF model of the BZ reaction develops a description of the reaction in terms of a set of differential equations containing only three variables. In common with experiments, the GF model shows both regular, intermittent and chaotic behavior. While remaining close to a real chemical system, it is sufficiently simple to allow detailed mathematical analysis [10]. The mechanism of the reaction is defined by the set of the following equations (1):

$$Y + X + H \rightarrow 2V \tag{1a}$$
$$Y + A + 2H \rightarrow V + H \tag{1b}$$
$$2X \rightarrow V \tag{1c}$$
$$0.5X + A + H \rightarrow X + Z \tag{1d}$$
$$X + Z \rightarrow 0.5X \tag{1e}$$
$$V + Z \rightarrow Y \tag{1f}$$
$$Z + M \rightarrow \tag{1g}$$

where the corresponding chemical components are: $Y = \mathrm{Br^-}$, $X = \mathrm{HBrO_2}$, $Z = \mathrm{Ce^{4+}}$, $V = \mathrm{BrCH(COOH)_2}$ or BrMA, $A = \mathrm{BrO_3^-}$, $H = \mathrm{H^+}$, $M = \mathrm{CH_2(COOH)_2}$. The concentrations of the main reactants A, H, M, and the total concentration of cerium ions C are summarized in Table 2.

3 Mathematical model

A three-variable mathematical model of the BZ reaction, presented by Györgyi and Field in [10], describes the reaction taking place in a CSTR. The corresponding set of nonlinear ordinary differential equations contains only three variables, while still being able to accurately reproduce the behavior of the BZ reaction observed experimentally [10] and it is based on a four-variable chemical mechanism (1), see [10].

The mathematical model, in its dimensionless form, consists of a set of scaled differential equations:

Table 2 Parameters of the investigated system (2).

List of parameters
$A = 0.1$
$M = 0.25$
$H = 0.26$
$C = 0.000833$
$\alpha = 666.7$
$\beta = 0.3478$

$$\frac{dx}{d\tau} = T_0(-k_1 H Y_0 x\tilde{y} + k_2 A H^2 Y_0/X_0\tilde{y} - 2k_3 X_0 x^2 + 0.5k_4 A^{0.5} H^{1.5} X_0^{-0.5}(C - Z_0 z)x^{0.5} - \\ - 0.5k_5 Z_0 xz - k_f x) \tag{2a}$$

$$\frac{dz}{d\tau} = T_0\left(k_4 A^{0.5} H^{1.5} X^{0.5}(C/Z_0 - z)x^{0.5} - k_5 X_0 xz - \alpha k_6 V_0 zv - \beta k_7 Mz - k_f z\right) \tag{2b}$$

$$\frac{dv}{d\tau} = T_0\left(2k_1 H X_0 Y_0/V_0 x\tilde{y} + k_2 A H^2 Y_0/V_0\tilde{y} + k_3 X_0^2/V_0 x^2 - \alpha k_6 Z_0 zv - k_f v\right) \tag{2c}$$

where $\tau = t/T_0$, $x = X/X_0$, $z = Z/Z_0$, $v = V/V_0$, and $\tilde{y} = \left(\alpha k_6 Z_0 V_0 zv/\left(k_1 H X_0 x + k_2 A H^2 + k_f\right)\right)/Y_0$ while t corresponding to time, X to $HBrO_2$, Y to Br^-, Z to Ce^{4+}, and V to BrMA. The rate constants and parameters used in the following computations are given in the Table 1 and 2, respectively.

The behavior of this system depends on the inverse residence time of the CSTR, the flow rate, noted k_f $[s^{-1}]$. As certain values of this parameter can give rise to chaos, the following analysis was performed in order to identify different dynamics.

4 Main results

The system of differential equations 2 was solved numerically in Matlab [18] using the *ode*45 solver. The simulations were done depending on free parameter k_f ranging from 3×10^{-4} to 5×10^{-4} with 10^{-7} step. Each simulation was performed for the final time $\tau = 100$ with a time step 10^{-4}. To avoid the systems distortions, only the last 20% of simulations were used for further computations. In all cases, initial conditions were set

$$x_0 = z_0 = v_0 = 1.$$

As a main results, phase diagrams, amplitude frequency spectrums (FFT), and Poincaré sections were done for relevant choices of the parameter k_f. To illustrate changes in dynamical behavior, bifurcation diagrams underlined by the approximate entropy and the 0-1 test for chaos with suitable magnifications to the parameter k_f were plotted.

Consequently, as a goal of this paper, bifurcation diagrams, the approximate entropy, and the 0-1 test for chaos were computed for nested set of parameters k_f. The 0-1 test for chaos splits the values of the parameter for which regular (periodic or quasi-periodic) and irregular (chaotic) movements appear, while the output of approximate entropy detects increasing complexity of the investigated system 2.

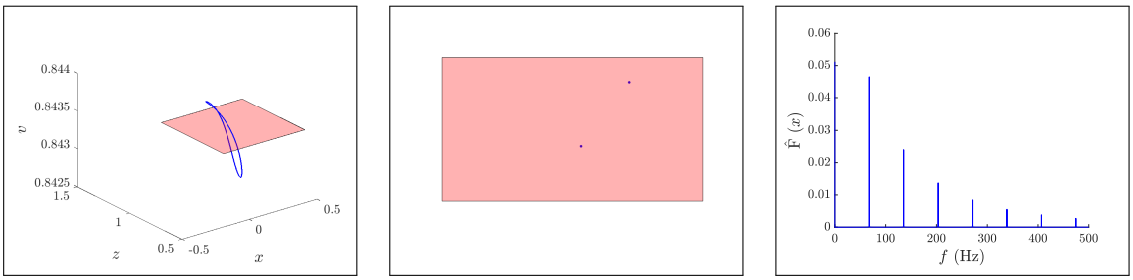

Fig. 1 Phase diagram with Poincaré section by plane $v = 0.8434$ and Fourier transform of variable x for $k_f = 3\times10^{-4}$.

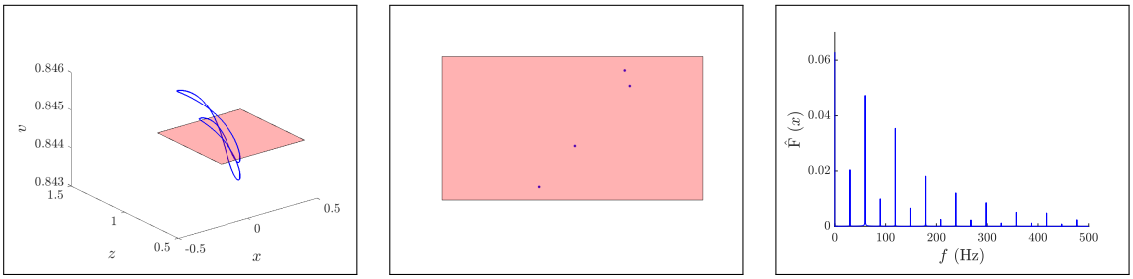

Fig. 2 Phase diagram with Poincaré section by plane $v = 0.8445$ and Fourier transform of variable x for $k_f = 3.2 \times 10^{-4}$.

4.1 Phase diagrams, the Fourier spectra, and bifurcation diagrams

Periodic as well as chaotic dynamics was identified in the studied model (2). For example, in Fig. 1 and Fig. 2, regular movement is shown by a trivial loop (Fig. 1) for $k_f = 3 \times 10^{-4}$, and a non-trivial loop (Fig. 2) for $k_f = 3.2 \times 10^{-4}$. Figure 3 gives an example of a chaotic trajectory, that is for $k_f = 3.5 \times 10^{-4}$.

The Fourier spectra were computed by Fast Fourier transform for $k_f = 3\times10^{-4}$, $k_f = 3.2\times10^{-4}$, and $k_f = 3.5 \times 10^{-4}$, shown in Figs. 1, 2, and 3 respectively. Regular behavior is observable for the first two and chaos in the last case.

In the case of regular movement, in Fig. 1 and Fig. 2, the Fourier spectra is formed by a number of harmonic frequencies, hence the frequency of the periodic trajectory is computable. Periodic motions of trajectory is also visible in Poincaré sections.

In the case of chaotic movement, Fig. 3, the Fourier spectra is formed by a number of harmonic components having the basic, super-harmonic, sub-harmonic, and combination frequencies on which further motions with frequencies forming the sided bands of the dominant frequencies are superposed. Their mutual ratio indicates the irregularity of the motion. The character of this chaotic motion is underlined by the Poincaré section.

Next, the bifurcation diagram (constructed as a projection of a local maxima) of the model (2) was plotted for each variable x, z and v with respect to the free parameter $k_f \in (3\times10^{-4}, 5\times10^{-4})$ in Figure 4. In this bifurcation diagram, so-called "period doubling" and "windows" effects are also visible. Periodic movement can be identified in the range of the parameter, e.g., $k_f \in (3\times10^{-4}, 3.24\times10^{-4})$ and $k_f \in (3.95\times10^{-4}, 5\times10^{-4})$. The interval in between these values is interrupted by chaotic cases around $k_f = 3.25$, and some $k_f \in (3.34\times10^{-4}, 3.65\times10^{-4})$ and $k_f \in (3.85\times10^{-4}, 3.9\times10^{-4})$.

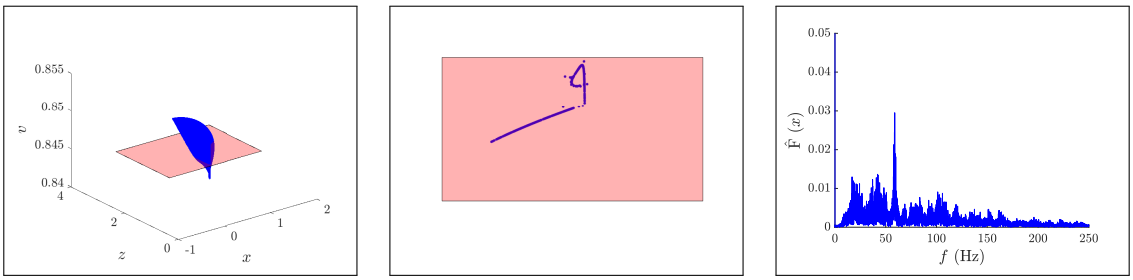

Fig. 3 Phase diagram with Poincaré section by plane $v = 0.847$ and Fourier transform of variable x for $k_f = 3.5{\times}10^{-4}$.

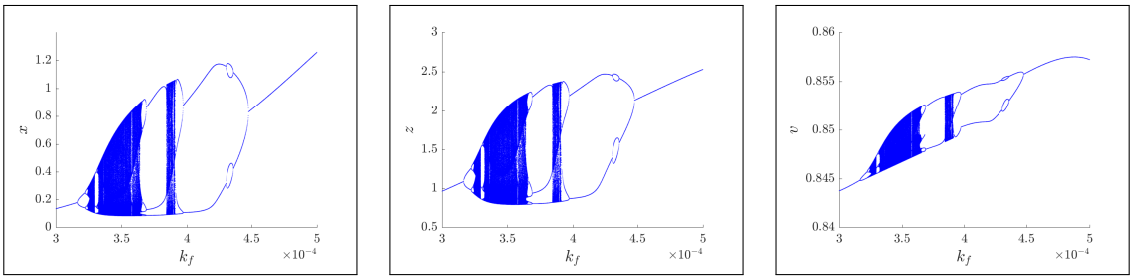

Fig. 4 Bifurcation diagram of the variable x(left), z(center), v(right) $k_f \in [3 \times 10^{-4}, 5 \times 10^{-4}]$.

4.2 Approximate entropy

The approximate entropy is a technique used to quantify the amount of regularity and unpredictability of fluctuations in time-series. The main advantages are that it can be computed on short time series and it allows to compare the differences in complexity of the same system with different parameters settings, see, e.g., [21] to be detected. More complex notion of entropy type can be found in, e.g., [14]. To compute the approximate entropy, two parameters must be set: embedding dimension m and neighborhood threshold r. Let $s(t) \in \mathbb{R}$ for $t = \{1, 2, \ldots, N\}$ be a time series with N observations. Then embedded vector $S(t)$ at time t, is defined as $S(t) = [s(t), s(t+1), s(t+2), \ldots, s(t+(m-1))]$, where t is the observed time and m is the embedding dimension. The maximum distance of embedded vectors is computed as follows:

$$D(i,j) = d(S(i), S(j)) = \max_{k=0,1,\ldots,m-1} |s(i+k) - s(j+k)|, \tag{3}$$

for $i, j = \{1, 2, \ldots, N-(m-1)\}$.

Compute the thresholded version of the distance with threshold given by r:

$$d_r(i,j) = \begin{cases} 1, & D(i,j) < r \\ 0, & otherwise, \end{cases} \tag{4}$$

for $i, j \in \{1, 2, \ldots, N-(m-1)\}$.

Compute $C_i^m(r)$ as a ratio between points in the neighborhood of i and the number of embedded vectors.

$$C_i^m(r) = \frac{\sum_{j=1}^{N-(m-1)} d_r(i,j)}{N-(m-1)}. \tag{5}$$

Then compute the average of logarithm of all the $C_i^m(r)$

$$\Phi^m(r) = \frac{1}{N-(m-1)} \sum_{i=1}^{N-(m-1)} \ln C_i^m(r). \tag{6}$$

Finally, approximate entropy for the finite time series with N data points is computed as

$$ApEn(m, r, N) = \Phi^m(r) - \Phi^{m+1}(r). \tag{7}$$

For robust estimation, it was suggested by Pincus [21] the time series is containing at least 10^3 observations.

The approximate entropy was calculated using the *TSEntropies* package [28] for R [27]. The computations were made for the input vector s given in a normalized form of all state variables:

$$s(t) = \sqrt{x^2(t) + z^2(t) + v^2(t)},$$

$k_f \in (3 \times 10^{-4}, 5 \times 10^{-4})$ and $r = 0.1$. The results of approximate entropy for all values of the parameter k_f are in Figs. 7–9.

4.3 0-1 test for chaos

The 0-1 test for chaos, invented by Gottwald and Melbourne [7], is one of the methods for distinguishing between regular and chaotic dynamics of a deterministic system. In contrast to the other approaches, the nature of the system is irrelevant, thus the test can be applied directly onto experimental data, ordinary differential equations, or partial differential equations. The results return values close to either 0 or 1, with 0 corresponding to regular dynamics and 1 to chaotic dynamics. With its easy implementation, evaluation, and wide range of application, using this tool for detecting chaos is becoming more popular in different fields.

The 0-1 test for chaos can be computed by the following algorithm [7].

Given the observation $\phi(j)$ for $j = 1, 2, ..., N$ and a suitable choice of $c \in (0, 2\pi)$, the following translation variables are computed:

$$p_c(n) = \sum_{j=1}^{n} \phi(j) \cos(jc),$$

$$q_c(n) = \sum_{j=1}^{n} \phi(j) \sin(jc)$$

for $n = 1, 2, ..., N$. The dynamics of the translation components p_c and q_c is shown on the p_c versus q_c plot. A bounded trajectory is in Fig. 5 (left) corresponding to regular movement, for $k_f = 3 \times 10^{-4}$. An unbounded trajectory is in Fig. 5 (right) related to the chaotic case, for $k_f = 3.5 \times 10^{-4}$.

The idea for the 0-1 test, first described in [7], is that the boundedness or unboundedness of the trajectory $\{(p_j, q_j)_{j \in [1,N]}\}$ can be studied through the asymptotic growth rate of its time-averaged mean square displacement (MSD), which is defined as

$$M(n) = \lim_{N \to \infty} \frac{1}{N} \sum_{j=1}^{N} d(j, n)^2$$

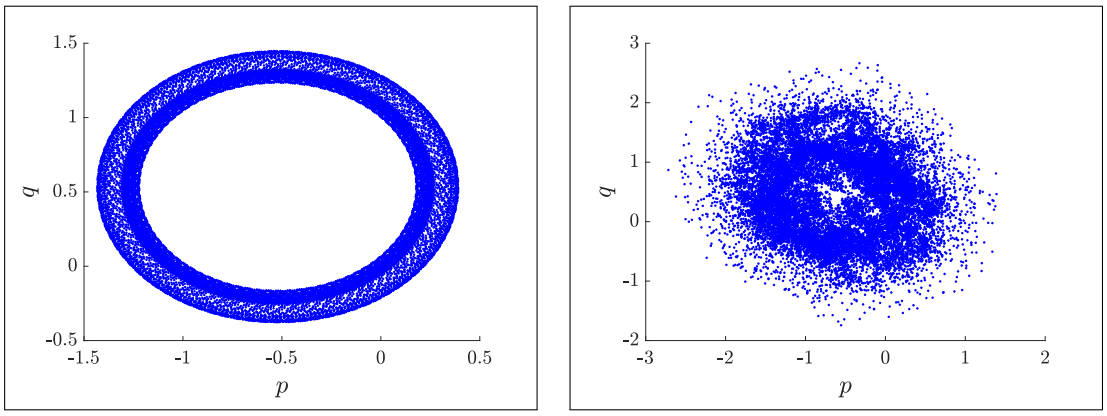

Fig. 5 The plot of p versus q for $c = 1.569853$ for $k_f = 3\times10^{-4}$ showing regular dynamics (left) and chaotic dynamics for $k_f = 3.5 \times 10^{-4}$(right).

where

$$d(j,n) = \sqrt{(p_{j+n} - p_j)^2 + (q_{j+n} - q_j)^2}$$

is the time lapse of the duration n ($n \ll N$) starting from the position at time j. As it is shown in [7,8], it is important to use values of n small enough compared to N, noted $n_{cut}, (n \leq n_{cut})$. A subset of time lags $n_{cut} \in [1, N/10]$ is advised for the computation of each K_c.

For bounded trajectories and regular dynamics, $M(n)$ is a bounded function in time, whereas unbounded trajectories, meaning chaotic dynamics, are described by $M(n)$ growing linearly with time. Thus the asymptotic growth rate of the MSD must be calculated, which correlates with the unboundedness of the trajectory.

As proposed in [7], the modified MSD is calculated as

$$D(n) = M(n) - E(\phi)^2 \frac{1 - \cos(nc)}{1 - \cos c}$$

The output of the 0-1 test for chaos is computed by the correlation method as

$$K_c = \mathrm{corr}(\xi, \Delta) \in [-1, 1]$$

for the vectors $\xi = (1, 2, ..., n_{cut})$ and $\Delta = (D_c(1), D_c(2), ..., D_c(n_{cut}))$.

The final result of the test is

$$K = \mathrm{median}(K_c).$$

The position of the studied system (2) at any moment of time is determined by displacements x, z, and v, which are used for defining vector ϕ:

$$\phi(j) = \sqrt{x(j)^2 + z(j)^2 + v(j)^2}.$$

For these simulations, a free software environment R [27] was used including the *Chaos01* package developed by T. Martinovič [17]. Comparison of values K_c for periodic and chaotic case is shown in Fig. 6, for $k_f = 3 \times 10^{-4}$ and $k_f = 3.5 \times 10^{-4}$, respectively.

The results of the 0-1 test for chaos for all values of the parameter k_f are in Figs. 7–9.

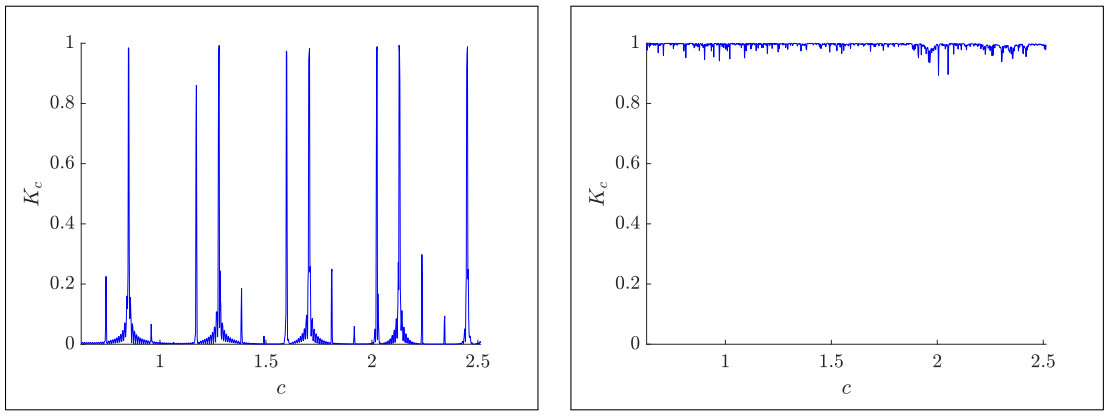

Fig. 6 The plot of K_c based on c for $k_f = 3 \times 10^{-4}$ showing regular dynamics (left) and for $k_f = 3.5 \times 10^{-4}$ showing chaotic dynamics (right).

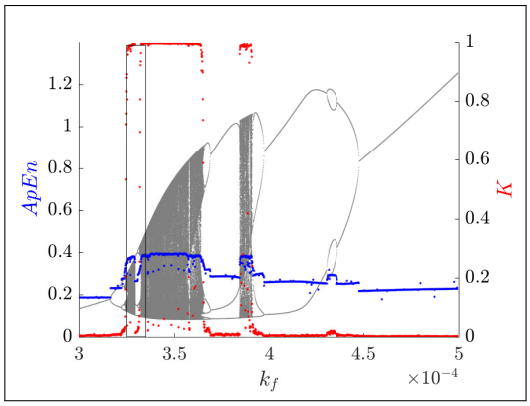

Fig. 7 The result of approximate entropy (in blue) and the result of the 0-1 test for chaos (in red) for $k_f \in (3 \times 10^{-4}, 5 \times 10^{-4})$. The magnification in the black rectangle is shown in Fig 8. The bifurcation diagram for variable x is shown in the background.

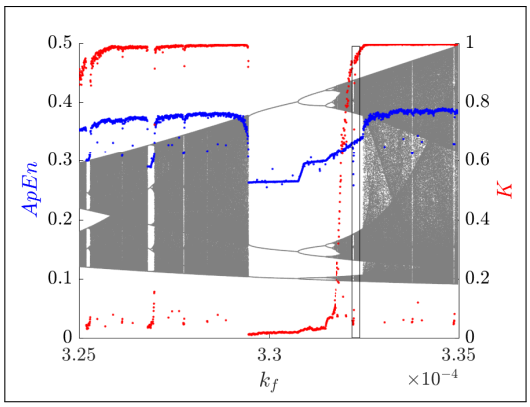

Fig. 8 The result of approximate entropy (in blue) and the result of the 0-1 test for chaos (in red) for $k_f \in (3.25 \times 10^{-4}, 3.35 \times 10^{-4})$. The magnification in the black rectangle is shown in Fig 9. The bifurcation diagram for variable x is shown in the background.

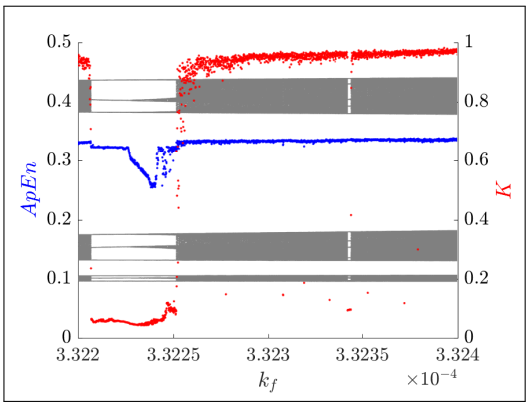

Fig. 9 The result of approximate entropy (in blue) and the result of the 0-1 test for chaos (in red) for $k_f \in (3.322 \times 10^{-4}, 3.324 \times 10^{-4})$. The bifurcation diagram for variable x is shown in the background.

5 Conclusions

In this paper, the GF model (2) associated with the BZ chemical reaction was solved using adaptive six-stage, fifth-order, Runge-Kutta method implemented as *ode*45 solver in Matlab. To eliminate the stiffness problem the model (2) was also simulated by *ode*23*s* solver in Matlab [18], outputs were identical.

The simulations were used to plot 3D phase portraits, bifurcation diagrams, the approximate entropy, and the 0-1 test for chaos. The mining process of dynamical properties were performed in the free software R [27] using packages *TSEntopies* [28] and *Chaos*01 [17] depending on flow rate parameter k_f.

It is evident from main results in Figs. 7–9 that both tests clearly detect regular and irregular patterns for given k_f. Our results show that the method of approximate entropy returns qualification constant which describes complexity in the system invariantly with respect to the origin. On the other hand, the 0-1 test as qualification tool returns zero for regular (periodic or quasi-periodic) movement and one for irregular (chaos) characteristics. Moreover, if the output of the 0-1 test is not close to zero or one, then the examined test case has not yet reached attractor or reached intermittent state, see e.g. [12] or [22] and references therein.

Further, we observe a correlation between approximate entropy and the 0-1 test for chaos. In general, the increasing values of the 0-1 test for chaos are coupled to increasing approximate entropy and vice versa.

We notice isolated low values of the 0-1 test for chaos accompanied by comparatively low values of approximate entropy well within of chaotic region characterized by high 0-1 test chaos values and approximate entropy. To investigate and zoom in, we have constructed three-stage system of nested subintervals of flow rates k_f, see Figs. 7–9, for which in every level the 0-1 test for chaos and approximate entropy was computed. At every level we observe the same pattern. That naturally yields suggestion of a fractal structure in the set of k_f:

Open Problem 1 *Is there a totally disconnected (Cantor) set of flow rates* k_f *in* $[3\times10^{-4}, 5\times10^{-4}]$ *such that for each such parameter the GF model* (2) *is showing chaos?*

Open Problem 2 *Is there a totally disconnected (Cantor) set of flow rates* k_f *in* $[3\times10^{-4}, 5\times10^{-4}]$ *such that for each such parameter the GF model* (2) *is showing regular movement?*

Acknowledgements This work was supported by The Ministry of Education, Youth and Sports from the National Programme of Sustainability (NPU II) project "IT4Innovations excellence in science – LQ1602"; by The Ministry of Education, Youth and Sports from the Large Infrastructures for Research, Experimental Development and Innovations project "IT4Innovations National Supercomputing Center – LM2015070"; by SGC grant No. SP2019/125 "Qualification and quantification tools application to dynamical systems", VŠB - Technical University of Ostrava, Czech Republic, Grant of SGS No. SP2019/84, VŠB - Technical University of Ostrava, Czech Republic.

References

1. A. Adamatzky, J. Holley, L. Bull, B. De Lacy Costello, Chaos Solitons Fractals 44, 779 (2011)
2. R. D'Ambrosio, M. Moccaldi, B. Paternoster, F. Rossi, J. Math. Chem. 56, 2876 (2018)
3. I.R. Epstein, J.A. Pojman, An Introduction to Nonlinear Chemical Dynamics: Oscillations, Waves, Patterns, and Chaos (Oxford University Press, 1998)
4. R.J. Field, E. Körös, R.M. Noyes, J. Am. Chem. Soc. 94, 8649 (1972)
5. R.J. Field, R.M. Noyes, J. Chem. Phys. 60, 1877 (1974)
6. P. Glansdorff, I. Prigogine, Thermodynamic Theory of Structure, Stability and Fluctuations (Wiley, 1971)
7. G.A. Gottwald, I. Melbourne, SIAM J. Appl. Dyn. Syst. 8, 129 (2009)
8. G.A. Gottwald, I. Melbourne, Nonlinearity 22, 1367 (2009)
9. L. Györgyi, R.J. Field, J. Phys. Chem. 95, 6594 (1991)
10. L. Györgyi, R.J. Field, Nature 355, 808 (1992)
11. L. Györgyi, S. L. Rempe, R. J. Field, J. Phys. Chem. 95, 3159 (1991)
12. J.F. Heagy, N. Platt, S.M. Hammel, Phys. Rev. E 49, 1140 (1994)
13. J.L. Hudson, M. Hart, D. Marinko, J. Chem. Phys. 71, 1601 (1979)
14. W. Jun, T. Lingyu, Z. Xianyong, L. Yuyan, Appl. Math. Nonlinear Sci. 2, 329 (2017)
15. H. Kang, Y. Pesin, Milan J. Math. 73, 1 (2005)
16. M. Lampart, T. Martinovič, J. Math. Chem. 57, 1670 (2019)
17. T. Martinovič, Chaos01: 0-1 Test for Chaos. (2016), https://CRAN.R-project.org/package=Chaos01. Accessed 1 October 2018
18. MATLAB 2015b (The MathWorks, Inc., 2015)
19. O.V. Noskov, A.D. Karavaev, V.P. Kazakov, S.I. Spivak, Mendeleev Commun. 4, 82 (1994)
20. C.V. Pao, J. Part. Diff. Eq. 1, 61 (1988)
21. S.M. Pincus, Proc. Natl. Acad. Sci. U.S.A. 88, 2297 (1991)
22. N. Platt, E.A. Spiegel, C. Tresser, Phys. Rev. Lett. 70, 279 (1993)
23. I. Prigogine, R. Lefever, J. Chem. Phys. 48, 1695 (1968)
24. W.H. Ruan, C.V. Pao, J. Math. Anal. Appl. 169, 157 (1992)
25. R.A. Schmitz, K.R. Graziani, J.L. Hudson, J. Chem. Phys. 67, 3040 (1977)
26. F. Schneider, Angew. Chem. 98, 941 (1986)
27. R: A Language and Environment for Statistical Computing (R Core Team, R Foundation for Statistical Computing, 2018)
28. J. Tomčala, TSEntropies: Time Series Entropies. (2018), https://CRAN.R-project.org/package=TSEntropies. Accessed 22 March 2019
29. J.J. Tyson, J. Phys. Chem. 86, 3006 (1982)
30. J.J. Tyson, in Lecture Notes in Biomathematics (Springer, 1994), p. 569
31. J.J. Tyson, P.C. Fife, J. Chem. Phys. 73, 2224 (1980)
32. H. Yamazaki, Y. Oono, K. Hirakawa, J. Phys. Soc. Jpn. 46, 721 (1979)